JOURNAL OF PETROLOGY | VOLUME 52 | NUMBERS 7 & 8 | PAGES 1415–1442 | 2011 | doi:10.1093/petrology/egr007

Monte Carlo Simulations of Metasomatic Enrichment in the Lithosphere and Implications for the Source of Alkaline Basalts

SÉBASTIEN PILET[1,2]*, MICHAEL B. BAKER[2], OTHMAR MÜNTENER[1] AND EDWARD M. STOLPER[2]

[1]INSTITUTE OF MINERALOGY AND GEOCHEMISTRY, UNIVERSITY OF LAUSANNE, 1015 LAUSANNE, SWITZERLAND
[2]DIVISION OF GEOLOGICAL AND PLANETARY SCIENCES, CALIFORNIA INSTITUTE OF TECHNOLOGY, PASADENA, CA 91125, USA

RECEIVED JUNE 18, 2010; ACCEPTED FEBRUARY 8, 2011
ADVANCE ACCESS PUBLICATION MARCH 31, 2011

One hypothesis for the origin of alkaline lavas erupted on oceanic islands and in intracontinental settings is that they represent the melts of amphibole-rich veins in the lithosphere (or melts of their dehydrated equivalents if metasomatized lithosphere is recycled into the convecting mantle). Amphibole-rich veins are interpreted as cumulates produced by crystallization of low-degree melts of the underlying asthenosphere as they ascend through the lithosphere. We present the results of trace-element modelling of the formation and melting of veins formed in this way with the goal of testing this hypothesis and for predicting how variability in the formation and subsequent melting of such cumulates (and adjacent cryptically and modally metasomatized lithospheric peridotite) would be manifested in magmas generated by such a process. Because the high-pressure phase equilibria of hydrous near-solidus melts of garnet lherzolite are poorly constrained and given the likely high variability of the hypothesized accumulation and remelting processes, we used Monte Carlo techniques to estimate how uncertainties in the model parameters (e.g. the compositions of the asthenospheric sources, their trace-element contents, and their degree of melting; the modal proportions of crystallizing phases, including accessory phases, as the asthenospheric partial melts ascend and crystallize in the lithosphere; the amount of metasomatism of the peridotitic country rock; the degree of melting of the cumulates and the amount of melt derived from the metasomatized country rock) propagate through the process and manifest themselves as variability in the trace-element contents and radiogenic isotopic ratios of model vein compositions and erupted alkaline magma compositions. We then compare the results of the models with amphibole observed in lithospheric veins and with oceanic and continental alkaline magmas. While the trace-element patterns of the near-solidus peridotite melts, the initial anhydrous cumulate assemblage (clinopyroxene ± garnet ± olivine ± orthopyroxene), and the modelled coexisting liquids do not match the patterns observed in alkaline lavas, our calculations show that with further crystallization and the appearance of amphibole (and accessory minerals such as rutile, ilmenite, apatite, etc.) the calculated cumulate assemblages have trace-element patterns that closely match those observed in the veins and lavas. These calculated hydrous cumulate assemblages are highly enriched in incompatible trace elements and share many similarities with the trace-element patterns of alkaline basalts observed in oceanic or continental setting such as positive Nb/La, negative Ce/Pb, and similiar slopes of the rare earth elements. By varying the proportions of trapped liquid and thus simulating the cryptic and modal metasomatism observed in peridotite that surrounds these veins, we can model the variations in Ba/Nb, Ce/Pb, and Nb/U ratios that are observed in alkaline basalts. If the isotopic compositions of the initial low-degree peridotite melts are similar to the range observed in mid-ocean ridge basalt, our model calculations produce cumulates that would have isotopic compositions similar to those observed in most alkaline ocean island basalt (OIB) and continental magmas after ~0·15 Gyr. However, to produce alkaline basalts with HIMU isotopic compositions requires much longer residence times (i.e. 1–2 Gyr), consistent with subduction and recycling of metasomatized lithosphere through the mantle. EM magmas cannot readily be explained without appealing to other factors such as a heterogeneous asthenosphere. These modelling results support the interpretation proposed by various researchers

*Corresponding author. E-mail: Sebastien.Pilet@unil.ch

© The Author 2011. Published by Oxford University Press. All rights reserved. For Permissions, please e-mail: journals.permissions@oup.com

that amphibole-bearing veins represent cumulates formed during the differentiation of a volatile-bearing low-degree peridotite melt and that these cumulates are significant components of the sources of alkaline OIB and continental magmas. The results of the forward models provide the potential for detailed tests of this class of hypotheses for the origin of alkaline magmas worldwide and for interpreting major and minor aspects of the geochemical variability of these magmas.

KEY WORDS: *alkali basalt; metasomatism; pyroxenite; hornblendite; oceanic lithosphere; continental lithosphere; modelling*

INTRODUCTION

Intraplate lavas from oceanic and continental settings range from highly nepheline (*ne*)-normative alkaline rock types such as nephelinites and basanites to hypersthene (*hy*)-normative tholeiites. They are generally characterized by fractionated incompatible trace-element contents that are higher, even at the tholeiitic end of the compositional range, than those found in mid-ocean ridge basalts (MORB) (Gast, 1968). Although aspects of the high trace-element contents of intraplate basalts can be explained by low degrees of partial melting of a garnet-peridotite source, the TiO_2 contents of oceanic island basalts (OIB) suggest that the sources of these lavas have TiO_2 concentrations higher than those estimated for primitive mantle (Prytulak & Elliott, 2007), which in turn suggests that other incompatible minor and trace elements may also be enriched in these sources. Such inferences for magma sources with trace-element enrichments relative to the primitive mantle are consistent with the need for trace-element enriched components in the sources of OIB to explain the range of their radiogenic isotopic compositions (Gast *et al.*, 1964; Chase, 1981; Hofmann & White, 1982; Zindler & Hart, 1986). This source enrichment has often been explained by the addition via subduction of recycled oceanic crust ± sediment (Chase, 1981; Hofmann & White, 1982; Palacz & Saunders, 1986; Hart, 1988; Nakamura & Tatsumoto, 1988; Barling & Goldstein, 1990; Weaver, 1991; Chauvel *et al.*, 1992). Alternatively, the enriched components could be metasomatized oceanic or continental lithospheric mantle (Sun & McDonough, 1989; Halliday *et al.*, 1992, 1995; Niu & O'Hara, 2003; Workman *et al.*, 2004; Pilet *et al.*, 2005, 2008; Panter *et al.*, 2006). Although these alternative hypotheses of crustal recycling vs metasomatized lithosphere are frequently considered to be mutually exclusive (Hofmann, 1997; Niu & O'Hara, 2003), both types of enriched components may play roles in the compositional and isotopic variability of the mantle sources of intraplate magmas (Workman *et al.*, 2004; Pilet *et al.*, 2008).

Highly alkaline magmas such as those in oceanic and continental intraplate volcanic systems cannot be produced by partial melting of dry (i.e. H_2O- and CO_2-free) mantle peridotite; if a peridotitic source is involved, generation of such magmas requires the presence of CO_2 (e.g. Eggler & Holloway, 1977; Wyllie, 1977; Dasgupta *et al.*, 2010). For example, results of melting experiments on CO_2-bearing peridotite suggest that the major-element compositions of alkaline magmas such as melilitites, nephelinites, and basanites can be produced by ~1–5% partial melting of a fertile peridotite with 0·1–0·25 wt % CO_2 (Hirose, 1997; Dasgupta *et al.*, 2007*a*). However, although the major-element compositions of alkaline magmas can be generated in this way, as emphasized above their trace-element contents require that their sources be enriched in trace elements above primitive mantle abundances (Prytulak & Elliott, 2007). An alternative process for generating highly alkaline magmas would be to melt silica-deficient lithologies such as olivine-bearing garnet pyroxenite (Hirschmann *et al.*, 2003; Keshav *et al.*, 2004; Kogiso *et al.*, 2004*a*; Dasgupta *et al.*, 2006) or hornblendite (Pilet *et al.*, 2008). However, an important aspect of the melting of these lithologies is that they are expected to melt to high degrees in plume settings (Hirschmann & Stolper, 1996; Ito & Mahoney, 2005*a*; Stolper & Asimow, 2007). Therefore, such source lithologies would themselves need to be highly enriched in incompatible trace elements [e.g. K, Rb, Ba, and light rare earth elements (LREE)] relative to peridotitic mantle to explain the high concentrations of these elements in alkaline magmas. As we show below, hornblendite veins in the lithosphere have this characteristic. Although known silica-deficient garnet pyroxenites do not typically have such enriched trace-element patterns, nor is typical recycled oceanic crust expected to be enriched in this way (Stracke *et al.*, 2003) (it should be noted that recycled oceanic crust is also generally viewed as incapable of generating highly nepheline-normative liquids upon partial melting), metasomatic processes for such enrichment can be envisioned (Bodinier *et al.*, 1987; Nielson & Noller, 1987; Wilshire, 1987; Harte *et al.*, 1993; Nielson & Wilshire, 1993).

Anhydrous veins rich in pyroxene and hydrous veins rich in amphibole and pyroxene are observed in mantle xenoliths and in obducted oceanic and continental lithospheric mantle (Varne, 1970; Conquéré, 1971, 1977; Best, 1974; Wilshire *et al.*, 1980; Menzies, 1983; Frey, 1983; Roden *et al.*, 1984; Vaselli *et al.*, 1995). These metasomatic veins are interpreted as cumulates formed during the percolation and differentiation of volatile-bearing melts within the lithosphere (Morris & Pasteris, 1987; Nielson & Noller, 1987; Wilshire, 1987; Harte *et al.*, 1993; Nielson & Wilshire, 1993; Downes, 2007). Melting experiments on amphibole-bearing veins indicate that high-degree melting of metasomatic veins followed by variable amounts of interaction with surrounding mantle can reproduce key features of the major- and trace-element compositions of alkaline

magmas (Pilet *et al.*, 2008). Two scenarios have been proposed for the production of alkaline magmas by melting of metasomatized lithosphere: (1) shortly after or coincident with metasomatism, the lithosphere experiences a thermal perturbation or decompression and melts *in situ* (Lloyd & Bailey, 1975; Wass & Rogers, 1980; Halliday *et al.*, 1990; Pilet *et al.*, 2008); or (2) metasomatized lithosphere is recycled into the convecting mantle by subduction or delamination and melts during later upwelling (e.g. in a plume; Halliday *et al.*, 1995; McKenzie & O'Nions, 1995; Niu & O'Hara, 2003; Pilet *et al.*, 2005, 2008). Both scenarios imply that alkaline magmas are produced by high degrees of melting (at least a few tens of per cent) of hydrous metasomatic veins or their dehydrated equivalents (Pilet *et al.*, 2008), and thus they require that the incompatible trace-element contents of the alkaline magmas primarily reflect the compositional characteristics of the metasomatic source material. This is an important aspect of the metasomatic model: some features considered diagnostic of intraplate alkaline magmas are simply inherited from their metasomatic source lithologies. Consequently, testing the metasomatic model requires evaluating whether these characteristics are indeed expected consequences of veins formed during the differentiation of low-degree volatile-rich mantle melts as they traverse the lithosphere.

To evaluate whether such metasomatic veins are a plausible consequence of metasomatism of the lithosphere, we constructed a forward model of vein formation and subsequent melting in the lithosphere. Although such petrogenetic modelling is typically done using inverse techniques (i.e. a model is specified and using available geochemical data the free parameters of the model are then solved for; e.g. Minster *et al.*, 1977; Minster & Allègre, 1978; Albarède, 1983, 1995; McKenzie & O'Nions, 1991), the sequential nature of the processes involved in metasomatic vein formation makes their modelling amenable to a forward approach. Because our forward modelling involves a large number of adjustable parameters with wide ranges of possible values (e.g. origin of the metasomatic fluid or melt, identity and proportions of crystallizing phases, trace-element partition coefficients, time delay between metasomatism and melting, etc.), we used Monte Carlo methods to investigate how the uncertainties on these parameters and their interplay affect the degree to which melting of metasomatized lithospheric sources is consistent with the trace-element contents and isotopic ratios of intraplate alkaline magmas.

BACKGROUND AND DESCRIPTION OF THE MODEL

Figure 1a shows schematically the model that we adopt here. The starting point is the generation of liquids by low degrees of partial melting at high pressures below a parcel of lithosphere. This could occur in a variety of environments, including small degrees of peripheral 'wet' melting during normal upwelling beneath a mid-ocean ridge (Halliday *et al.*, 1995; Class & Goldstein, 1997; Niu & O'Hara, 2003) (Fig. 1a), in front or at the periphery of an ascending mantle plume beneath continental or oceanic lithosphere (Wyllie, 1988*a*, 1988*b*; Halliday *et al.*, 1995) (Fig. 1b), or as a result of upwelling of the asthenosphere beneath rifting lithosphere (Lloyd & Bailey, 1975; Wass & Rogers, 1980; Pilet *et al.*, 2004; Thompson *et al.*, 2005) (Fig. 1c). These low-degree melts then ascend into the lithosphere and interact both chemically and thermally with their surroundings: Chemical interactions lead to both cryptic and modal metasomatism of the peridotitic country rock, and thermal interactions result in the formation of veins as the ascending melts lose heat to the country rock and crystallize (Bodinier *et al.*, 1987; Morris & Pasteris, 1987; Nielson & Noller, 1987; Wilshire, 1987; McKenzie, 1989; Harte *et al.*, 1993). Alkaline melts then form by melting of the assemblage of veins and metasomatized peridotite.

Origin and crystallization of the metasomatic liquid

Metasomatic veins are interpreted as cumulates formed during the fractional crystallization of volatile-rich melts within the lithosphere (Morris & Pasteris, 1987; Nielson & Noller, 1987; Wilshire, 1987; Harte *et al.*, 1993; Nielson & Wilshire, 1993; Downes, 2007). Although the compositions of the melts that produce metasomatic veins in the lithosphere are poorly constrained, they are generally thought to be low-degree partial melts of $H_2O + CO_2$-bearing mantle peridotite. Ascent, reaction, cooling, and fractional crystallization of these low-degree melts in the lithospheric mantle generates a continuum of phase assemblages ranging from anhydrous [dominantly clinopyroxene (cpx) + garnet (gt) ± olivine (ol) ± orthopyroxene (opx)] to hydrous [dominantly amphibole (amph) + cpx ± phlogopite (phlog) ± opx] veins enriched in highly incompatible elements, plus a modal and cryptic enrichment in the surrounding peridotite (Morris & Pasteris, 1987; Nielson & Noller, 1987; Wilshire, 1987; Bodinier *et al.*, 1990; Harte *et al.*, 1993; Nielson & Wilshire, 1993). Low-degree partial melts of peridotite at pressures corresponding to the base of the lithosphere (~2–3·5 GPa) are expected to be highly *ne*-normative if the dominant volatile species is CO_2 (Hirose, 1997; Dasgupta *et al.*, 2007*a*) or *hy*-normative if the volatile component is dominated by H_2O (Hirose & Kawamoto, 1995; Gaetani & Grove, 1998; Grove *et al.*, 2006). However, fractional crystallization experiments on both *hy*- and *ne*-normative hydrous basaltic liquids (Nekvasil *et al.*, 2004; Pilet *et al.*, 2010) at pressures of ~0·9–1·5 GPa indicate that the crystallizing assemblages are broadly similar: clinopyroxene + minor olivine at high temperatures and amphibole + minor clinopyroxene at

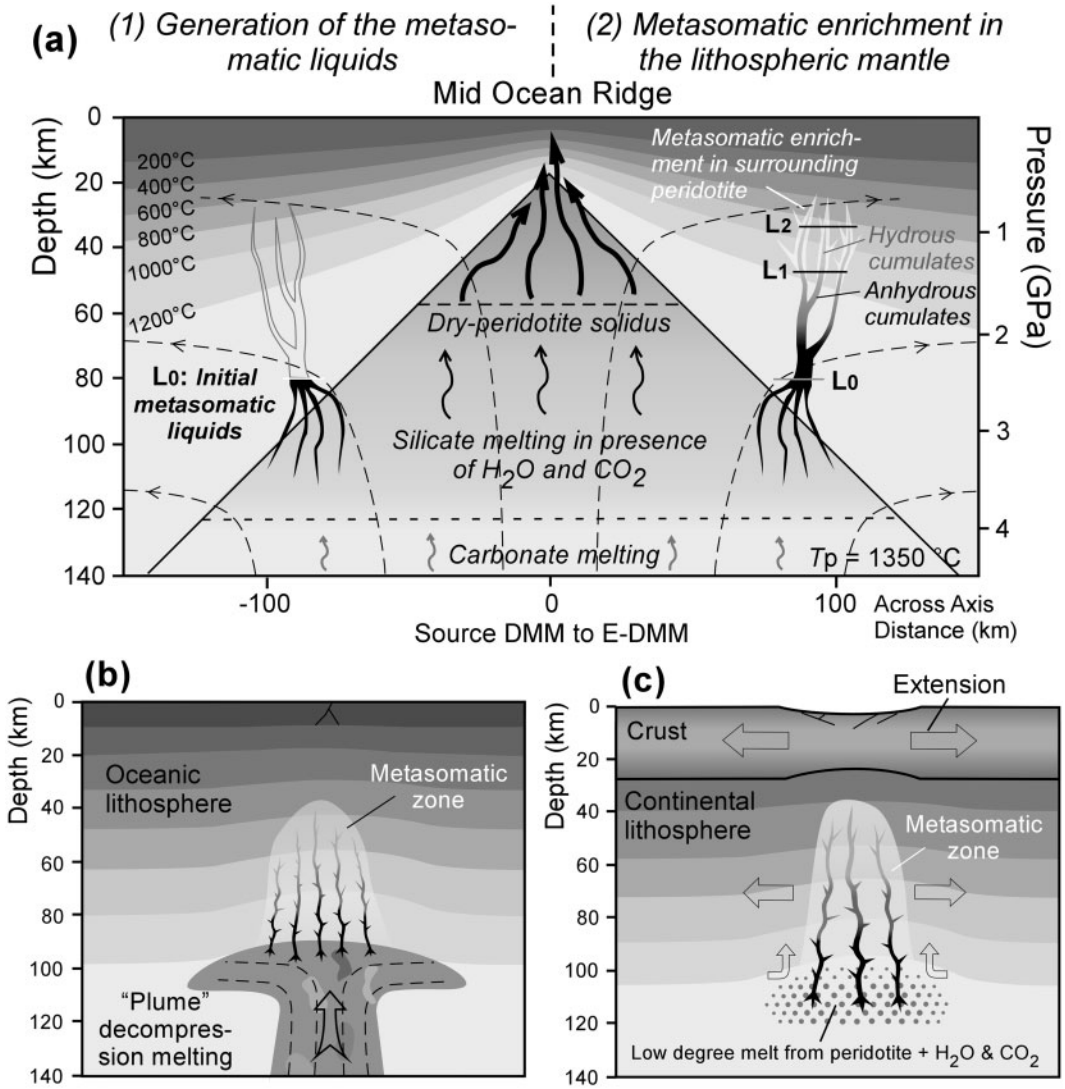

Fig. 1. (a) Schematic model for lithospheric metasomatism at the periphery of a mid-ocean ridge. This model is based on models suggested by Halliday *et al.* (1995) and Niu & O'Hara (2003). It assumes that some near-solidus liquids produced at depth in the melting column are not collected to form MORB, but percolate across the cooling lithosphere and generate anhydrous and hydrous cumulate veins plus cryptic and modal metasomatic enrichment in the adjacent peridotite. The geometry and thermal structure of the cooling lithosphere is based on the model published by Shaw *et al.* (2010) for the Gakkel Ridge. (b) Schematic model for the metasomatism of the oceanic lithosphere induced by a mantle plume. Some melts produced by plume upwelling do not reach the surface but percolate through and differentiate within the oceanic lithosphere producing anhydrous and hydrous cumulates plus metasomatic enrichment in the lithospheric peridotite surrounding these cumulates (Wyllie, 1988*a*, 1988*b*; Halliday *et al.*, 1995). (c) Schematic model for the metasomatism of the continental lithosphere. The generation of asthenospheric melts responsible for the formation of metasomatic veins and cryptic and modal metasomatism in adjacent peridotite surrounding the veins is due to upwelling of the asthenosphere beneath rifting lithosphere (Lloyd & Bailey, 1975; Wass & Rogers, 1980; Pilet *et al.*, 2004; Thompson *et al.*, 2005) or to 'finger-like' plumes (Granet *et al.*, 1995; Hoernle *et al.*, 1995; Wilson & Patterson, 2001). (See the text and Fig. 4 for a discussion of L_0, L_1, and L_2, and for the gray-scale coding of the schematic veins.)

lower temperatures. In addition, amphiboles that crystallize in experiments on *ne*- and *hy*-normative liquids at these pressures are similar in major-element composition (including Ti, Na, and K) to amphiboles observed in lithospheric veins worldwide (Pilet *et al.*, 2010). Based on these observations, we assume in our modelling that (1) the assemblage that crystallizes from a low-degree melt of peridotite is insensitive to whether the melt is *ne*- or *hy*-normative, and (2) the formation of amphibole cumulates similar in composition to those found in metasomatic veins can be produced by the differentiation of a liquid similar to those produced by partial melting of peridotite

with a volatile content representative of the Earth's upper mantle regardless of whether the liquid is *ne*- or *hy*-normative.

Water concentration in the metasomatic liquid

We assume that the melt that metasomatizes the lithosphere is produced at pressures within the garnet-lherzolite field and at temperatures between the dry solidus and the vapor or fluid-saturated solidus (Fig. 1a). The presence of several hundred ppm H_2O or CO_2 in the mantle significantly decreases the the temperature at which the melting of peridotite begins, and several models provide a basis for calculating the effect of volatiles on the solidus temperature (Hirth & Kohlstedt, 1996; Katz *et al.*, 2003; Asimow *et al.*, 2004; Aubaud *et al.*, 2004; Dasgupta *et al.*, 2007*b*). For example, Fig. 2a shows the melting behaviour of depleted MORB mantle (DMM) calculated for a potential adiabat temperature of 1350°C using the parameterization of Dasgupta *et al.* (2007*b*) for peridotite melting in the presence of 110 ppm H_2O and 36 ppm CO_2, the average volatile contents estimated by Workman & Hart (2005) for DMM. The extremely low degrees of melting (>0·15 wt %) calculated for the depth interval corresponding to 2·5–3 GPa (the gray line in Fig. 2a) suggest that, for the assumed adiabat temperature, these volatile contents are too low to produce sufficient melt to metasomatize the lithosphere. A number of studies have shown that the H_2O (and CO_2) contents of the Earth's mantle can be variable (Michael, 1995; Sobolev & Chaussidon, 1996; Dixon *et al.*, 2002; Saal *et al.*, 2002; Simons *et al.*, 2002; Pineau *et al.*, 2004; Aubaud *et al.*, 2005; Macpherson *et al.*, 2005; Cartigny *et al.*, 2008; Hirschmann & Dasgupta, 2009). Given this variability, we have also calculated the isentropic melting behaviour of peridotitic mantle containing 300 and 90, 400 and 120, and 500 and 150 ppm H_2O and CO_2, respectively (the black lines in Fig. 2a) using the same adiabat temperature (1350°C). It should be noted that a source with 400 ppm H_2O and 120 ppm CO_2 has an H/C mass ratio of 0·75, similar to the estimate of DMM (Hirschmann & Dasgupta, 2009). Such volatile contents are able to produce low-degree melts at significantly greater depths than for dry melting and more importantly, the fraction of melt is significantly greater than for the case with the lower volatile contents discussed above. It is likely that in this case, the melt is sufficiently abundant to represent a viable agent for the metasomatism of the cooling lithosphere as proposed by Halliday *et al.* (1995) and Niu & O'Hara (2003). The black model melting curves in Fig. 2a yield a degree of melting (F) ranging from <0·2 wt % at 4 GPa to ~2 wt % at ~2·2–2·6 GPa. It should be noted that such melts will contain significant amounts of H_2O: for example, a 0·75% partial melt generated at ~2·8 GPa from a source containing 400 ppm H_2O and 120 ppm CO_2 will contain ~2·43 wt % H_2O and ~1·53 wt % CO_2 [using a simple batch melting equation and bulk peridotite/melt D values for H_2O and CO_2 of 0·009 and 0·0001, respectively (Aubaud *et al.*, 2004; Shcheka *et al.*, 2006)]. A relatively high concentration of water in the initial partial melt is important for the model that we are evaluating as its success requires that amphibole crystallizes from the metasomatic liquids as they move through the lithosphere; this amount of water coupled with 40–50% anhydrous crystallization will in turn yield residual liquids with >3 wt % H_2O, which seems sufficient to stabilize amphibole (Sisson & Grove, 1993; Nekvasil *et al.*, 2004) under lithospheric conditions.

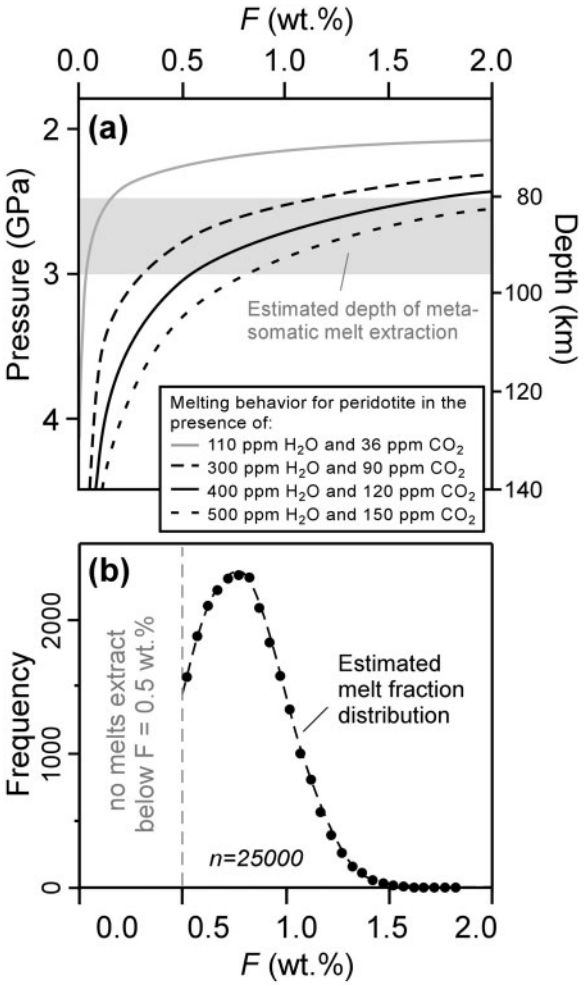

Fig. 2. (a) Relationship between depth and melt fraction (F) for isentropic melting of peridotites containing various amounts of H_2O and CO_2. These melting curves are calculated based on the parameterization of Dasgupta *et al.* (2007*b*) for the combined effect of H_2O and CO_2 on peridotite melting temperatures and using a potential adiabat temperature of 1350°C. The gray band shows our estimate for the depths of metasomatic melt extraction. (b) Frequency distribution of melt fraction for asthenospheric melting used in our Monte Carlo simulations.

Parameters of the model

The first two steps in the model are (1) formation of a low-degree partial melt of a volatile-bearing garnet peridotite, and (2) differentiation of this liquid as it moves through the lithosphere, generating different cumulate assemblages as it ascends and cools. The parameters describing these processes are discussed below and all have associated uncertainties. We have estimated both the parameters and their uncertainties using experimental, petrological, and geochemical constraints and have used Monte Carlo simulations to understand how these uncertainties propagate through the calculation and affect the calculated compositions of the potential metasomatic sources of alkaline magmas.

Partial melting of asthenospheric peridotite in the presence of H_2O–CO_2

Our assumptions and inputs to the model for the origin of the low-degree melts that metasomatize the lithosphere are as follows (it should be noted that in the discussion that follows, C_s denotes the trace-element concentration in the asthenospheric source and F is the degree of partial melting of that source).

(1) The trace-element composition of the asthenospheric source of the low-degree mantle melt is assumed to span a range similar to that of the sources of typical MORB. We thus allow its composition to vary between DMM and enriched (E)-DMM as calculated by Workman & Hart (2005). Wider ranges (both more depleted and more enriched) can be envisioned, but at this point we prefer to use a well-constrained and documented approach for estimating the composition of the asthenospheric mantle.

(2) To estimate variations in the degree of partial melting of the asthenosphere, we have used calculated melting curves for peridotite sources containing 300–400 ppm H_2O and 90–120 ppm CO_2 (Fig. 2a). We assume that these near-solidus melts are extracted from the source at pressures between 3 and 2·5 GPa (corresponding to ~100–80 km depth); this corresponds to a variation in the degree of partial melting of the asthenospheric source from ~0·3 wt % at 3 GPa for a source with 300 ppm H_2O and 90 ppm CO_2 to ~1·8 wt % at 2·5 GPa for a source with 400 ppm H_2O and 120 ppm CO_2. To reproduce this range in our model, we generated a Gaussian distribution for the degree of partial melting with a mean of 0·75 wt % and a standard deviation of 0·25 wt % (Fig. 2b). Tests applying a flat distribution to the degree of melting of the source show that the results are independent of the type of distribution chosen; the average and the range of liquid compositions are similar, only the standard deviation increases slightly when a flat distribution is used. Because the threshold below which basaltic liquids remain trapped in a peridotite source is still in debate (McKenzie, 1989; Lundstrom *et al.*, 1995; Faul, 2001), we arbitrarily truncated our Gaussian at 0·5 wt % melt (Fig. 2b). It should be noted that this truncation skews metasomatic liquid compositions to lower trace-element contents, in the opposite direction to what one might want to explain the formation by differentiation of trace-element rich metasomatic cumulates.

(3) Our choice of the pressures of melt extraction and a potential adiabat temperature of 1350°C places melting mostly in the garnet-stability field (Robinson & Wood, 1998); the melting mode from the 3 GPa experiments of Walter (1998) is used as an input in the accumulated non-modal fractional melting equation (solidus phase proportions and melting mode are reported in Table 1). Figure 2a suggests that melt percentages > ~1% are derived at pressures of 2·8–2·5 GPa; that is, close to or within the spinel-peridotite field. We have not included the garnet to spinel transition in our melting calculation, and thus for melting percentages of ~1–1·8 wt %, the calculated heavy REE (HREE) content of our model partial melt would be slightly low relative to a model liquid calculated for a spinel-lherzolite assemblage. The selected trace-element partition coefficients ($D^{min/liq}$) are reported in Table 2, and Fig. 3 shows a comparison between the $D^{min/liq}$ values used in our model and other published distribution coefficients for the same set of phases.

Fractionation of the metasomatic liquid within the lithosphere

We assume that the near-solidus melt begins to crystallize in magma channels once it migrates into the lithosphere. We neglect the compositional effects of chemical interaction between the melt and the wall-rock. The consequence of this assumption on the crystallization sequence of the melt is unknown, but for incompatible trace elements, the differences between the metasomatic liquids and peridotite are so high that the effects of wall-rock interaction on the trace-element contents of the melts or their cumulates are expected to be minor. Lacking specific experimental constraints on polybaric differentiation of volatile-bearing near-solidus melts of peridotite at lithospheric pressures, we have estimated a differentiation trend based on available experimental basaltic liquid lines of descent at lithospheric pressures (Müntener *et al.*, 2001; Nekvasil *et al.*, 2004; Müntener & Ulmer, 2006; Pilet *et al.*, 2010), on the high-pressure experiments of Hack *et al.* (1994) and Hauri *et al.* (1994), and on the observed mineral assemblages in metasomatic veins (Irving, 1974; Lloyd & Bailey, 1975; Wass & Rogers, 1980; Wilshire *et al.*, 1980;

Table 1: Modal abundances in DMM and E-DMM sources and melting mode

	Ol	Cpx	Opx	Gt	Sulfide*
Modal abundances†	0·59	0·11	0·19	0·11	0·00037
Melting mode‡	0·07	0·68	−0·16	0·25	0·0037

*MORB and OIB compositions suggest that Pb has a bulk *D* similar to that of Ce—significantly more compatible than would be predicted for a garnet- or spinel-lherzolite source given single silicate mineral–liquid *D* values for Pb (Hofmann *et al.*, 1986). This higher apparent compatibility of Pb during partial melting may reflect the presence of minor residual sulphides in the OIB and MORB sources (Sims & DePaolo, 1997; Hart & Gaetani, 2006). To produce low-degree melts with Ce/Pb ratios similar to the ratios observed in enriched MORB (~15–35; Salters & Stracke, 2004), we added 0·037% sulfide to the mantle source [equal to ~128 ppm S; this is slightly higher than the DMM estimate of 119 ppm (Salters & Stracke, 2004), but there are no S estimates for E-DMM]. We assume that the sulphide is removed from the source after 10% partial melting.
†Modal abundances of the four silicate phases are based on the major-element composition of DMM (Workman & Hart, 2005) and the model of Baker *et al.* (2008) for estimating peridotite modal proportions. In the calculations, both the modal abundances and the melting mode (i.e. the sum of ol + cpx + gt + sulfide) equal unity.
‡Silicate-phase melting mode for a garnet peridotite at 3 GPa from Walter (1998).

Bodinier *et al.*, 1987; Morris & Pasteris, 1987; Nielson & Noller, 1987; Wilshire, 1987; Harte *et al.*, 1993; Wulff-Pedersen *et al.*, 1999; Downes, 2007; Lorand & Gregoire, 2010). The crystallization sequence and mineral proportions in the cumulates shown in Fig. 4 are based on these experiments and petrological observations. With decreasing pressure (~2·5 to ~0·8 GPa) and temperature (~1300°C to ~800°C) the cumulate assemblages are assumed to be clinopyroxene ± garnet ± olivine ± minor orthopyroxene, followed at lower temperatures by a hydrous cumulate assemblage dominated by amphibole ± clinopyroxene ± minor orthopyroxene, garnet, phlogopite, and plagioclase (pl) (which appears only if the pressure is below ~1 GPa; Nekvasil *et al.*, 2004). It should be noted that the depth (or pressure) range of magma crystallization will depend on a range of unknown factors (e.g. the temperature contrast between the melt and country rock; the geometry of the conduits and the melt flux; the temperature profile of the lithosphere; whether the lithosphere is oceanic or continental; etc.); nevertheless, we assume that the anhydrous cumulates form at pressures between ~2·5 and ~1·5 GPa, and that the hydrous cumulates crystallize at slightly lower pressures (~2 to ~0·8 GPa).

The ranges in the proportions of the phases used in our Monte Carlo simulations are listed in Fig. 4. We explain here several aspects of the procedures and assumptions by which crystallization of these phases, their proportions, and partition coefficients were applied.

(1) Experimental constraints on basaltic magma fractionation at high pressure indicate that for pressures >2·0 GPa, the anhydrous cumulates are clinopyroxene + garnet (Hack *et al.*, 1994; Hauri *et al.*, 1994), but at lower pressure (<1·5 GPa) the cumulate assemblage switches to clinopyroxene + minor olivine (Nekvasil *et al.*, 2004; Pilet *et al.*, 2010). Therefore, we linked the proportions of garnet and olivine crystallizing in the deepest lithospheric zone (i.e. between L_0 and L_1; Fig. 4) to avoid anhydrous cumulates rich in olivine and garnet, which are not observed in experimental studies or in natural anhydrous metasomatic veins.

(2) Although the crystallization of accessory minerals has little effect on the major-element composition of a liquid (with the possible exception of Fe–Ti oxides and titanite), these minerals (as cumulates) can control the concentrations of a number of incompatible trace elements in the metasomatic veins. Based on descriptions of hydrous metasomatic veins in the literature (Wass & Rogers, 1980; Lloyd, 1981; Bodinier *et al.*, 1987, 1996; Zanetti *et al.*, 1996; Wulff-Pedersen *et al.*, 1999; Pilet *et al.*, 2008; Lorand & Gregoire, 2010) and petrographic study of amphibole-bearing veins from the French Pyrenees, we included the following accessory minerals in our calculation: titanite, ilmenite, rutile, allanite, apatite, sulphide, and zircon. Although expressions exist for calculating the saturation surfaces for rutile (Gaetani *et al.*, 2008), apatite (Pichavant *et al.*, 1992), and zircon (Hanchar & Watson, 2003) in silicate melts, these expressions require, in addition to temperature, the major-element composition of the liquid, which we cannot calculate at present. At constant liquid composition, the ZrO_2 content required for zircon saturation decreases with decreasing temperature (Hanchar & Watson, 2003) and thus we assume zircon crystallizes only from relatively low-temperature, differentiated melts. Therefore, we postulate two stages of hydrous vein formation: a first stage where zircon is absent and a second stage where minor zircon could crystallize. This second stage is also characterized by the presence of minor plagioclase, which is observed after ~75% crystallization in experiments that simulate the incremental fractional crystallization of a hawaiite at 0·93 GPa (Nekvasil *et al.*, 2004).

(3) All parameters listed in Fig. 4 were allowed to vary within their specified ranges based on flat distributions (i.e. all values in the specified range have equal

Table 2: Mineral–liquid distribution coefficients ($D^{min/liq}$) used in the calculations

	Rb	Ba	Th	U	Nb	La	Ce	Pb	Pr	Sr	Nd	Sm
Olivine	0·00018	0·0003	0·00001	0·0004	0·005	0·0004	0·0005	0·00001	0·001	0·00019	0·001	0·001
Clinopyroxene	0·0007	0·00068	0·0008	0·0008	0·0077	0·0536	0·0858	0·01	0·1	0·13	0·19	0·29
Orthopyroxene	0·0006	0·001	0·00	0·00	0·0031	0·002	0·003	0·0013	0·0048	0·007	0·0068	0·01
Garnet	0·0007	0·0007	0·0015	0·005	0·02	0·01	0·021	0·0005	0·045	0·006	0·087	0·217
Amphibole	0·10	0·36	0·018	0·016	0·53	0·23	0·40	0·096	0·63	0·69	0·91	1·39
Phlogopite	3	4	0·01	0·01	0·6	0·05	0·055	0·2	0·06	0·3	0·065	0·07
Plagioclase	0·2	0·6	0·07	0·11	0·05	0·27	0·2	0·36	0·17	3	0·14	0·11
Ilmenite	0·004	0·007	0·008	0·027	13·3	0·01	0·013	0·93	0·02	0·04	0·03	0·06
Titanite	0·0014	0·0024	10·0	6·6	20·0	10·6	15·9	0·1	25·0	0·35	33·9	48·0
Apatite	0·006	0·021	11·25	12·00	0·05	16·9	20·8	0·13	22·0	5·3	25·1	28·3
Zircon	0·006	0·004	44	250	230	0·2	1	0·1	2·5	0·03	0·6	3
Rutile	0·01	0·01	0·5	0·5	83·4	0·30	0·25	0·22	0·20	0·15	0·10	0·08
Allanite	0·01	0·01	803	56·3	0·2	1598	1278	2·8	1200	0·6	1115	746
Sulfide	0·0001	0·0001	0·0001	0·0001	0·0001	0·0001	0·0001	10*	0·0001	0·0001	0·0001	0·0001

	Zr	Hf	Eu	Ti	Gd	Tb	Dy	Ho	Y	Er	Yb	Lu
Olivine	0·010	0·005	0·002	0·020	0·002	0·002	0·002	0·002	0·005	0·002	0·0015	0·0015
Clinopyroxene	0·12	0·26	0·47	0·38	0·48	0·48	0·44	0·42	0·4	0·39	0·43	0·43
Orthopyroxene	0·01	0·01	0·013	0·024	0·016	0·019	0·022	0·026	0·028	0·03	0·049	0·06
Garnet	0·32	0·32	0·4	0·2	0·498	0·75	1·06	1·53	2·11	3	4·03	5·5
Amphibole	0·43	0·72	1·44	2·50	1·65	1·62	1·58	1·54	1·48	1·34	1·10	1·10
Phlogopite	0·08	0·08	0·09	3	0·095	0·1	0·1	0·1	0·1	0·1	0·1	0·1
Plagioclase	0·03	0·03	0·73	0·04	0·066	0·06	0·055	0·048	0·06	0·041	0·031	0·025
Ilmenite	0·02	0·08	0·14	50 wt %†	0·14	0·14	0·19	0·16	0·14	0·27	0·19	0·18
Titanite	4·5	7·3	44·2	39·5 wt %†	55·0	50·0	48·4	45·0	43·0	37·4	30·3	22·8
Apatite	0·02	0·02	17·0	0·02	21·3	20·4	19·5	18·7	16·9	13·8	8·5	7·8
Zircon	65 wt %†	1 wt %†	3	0·1	6·5	26	45	70	80	90	100	110
Rutile	5·95	7·08	0·050	98·5 wt %†	0·040	0·035	0·028	0·022	0·018	0·015	0·012	0·01
Allanite	0·1	0·2	507	2·8	200	150	100	70	50	45	30	20
Sulfide	0·0001	0·0001	0·0001	0·0001	0·0001	0·0001	0·0001	0·0001	0·0001	0·0001	0·0001	0·0001

These mineral–liquid *D* values are plotted as filled red circles in Fig. 3. It should be noted that these values are not simply averages of the available data plotted in Fig. 3. For certain phases (e.g. clinopyroxene) we have used the values from a single study (Hart & Dunn, 1993), whereas for amphibole we have used the averages of values from Tiepolo *et al*. (2000*a*, 2000*b*, 2007). For other phases we have averaged *D* values 'by eye' in that we have been guided by the data plotted in Fig. 3, but have attempted to maintain the relative fractionations between different elements for a given phase that can be seen qualitatively in Fig. 3. Because for some phases some *D* values have been determined many more times than those for their adjacent elements, simple averaging does not necessarily maintain these relative fractionations.
*Pb $D^{sulfide/silicate\ liquid}$ from Halliday *et al*. (1995).
†For titanite, ilmenite, and rutile, wt % TiO_2 contents rather than *D* values were used to calculate the effect of the fractionation of these phases on model cumulate or residual liquid compositions; for zircon, wt % ZrO_2 and HfO_2 contents were used [the zircon HfO_2 content was estimated using data compiled by Hoskin & Schaltegger (2003)].

probability). With the exception of Ti-rich phases (ilmenite, rutile, and titanite) and zircon, we then used the fractional crystallization equation and the $D^{min/liq}$ values listed in Table 2 to calculate the trace-element contents of the residual liquids and cumulates as a function of melt fraction. For ilmenite, rutile, titanite, and zircon, we used stoichiometric compositions rather than $D^{min/liq}$ values for calculating the effect of these fractionating phases on Ti, Zr, and Hf contents [a Hf content of 1 wt % in zircon

was estimated using data compiled by Hoskin & Schaltegger (2003) on various igneous rocks].

As observed in outcrop and in veined xenoliths, modally and/or cryptically metasomatized peridotite is often associated with amphibole-bearing metasomatic veins (Bodinier *et al.*, 1990; Nielson & Wilshire, 1993; Nielson *et al.*, 1993; McPherson *et al.*, 1996; Woodland *et al.*, 1996; Zanetti *et al.*, 1996; Wulff-Pedersen *et al.*, 1999). As illustrated in Fig. 4b, this metasomatism can include phlogopite-rich veinlets infiltrating the surrounding peridotite and thin glass 'films' along grain boundaries and interstitial 'glass pockets' within the peridotite (e.g. Wulff-Pedersen *et al.*, 1999). In addition to direct infiltration of melt, a reaction zone (consisting of ol, Cr-rich cpx, opx, amph, and phlog) is often observed within peridotite that is in direct contact with amphibole-bearing veins (Wilshire *et al.*, 1980; Bodinier *et al.*, 1990, 2004; McPherson *et al.*, 1996; Woodland *et al.*, 1996; Zanetti *et al.*, 1996; Wulff-Pedersen *et al.*, 1999). Such cryptic and modally metasomatized peridotites are incompatible-trace-element enriched relative to far-field peridotites, and if they were to melt owing to the same perturbations that lead to melting of the associated metasomatic veins, they could also contribute a trace-element enriched component to magmas derived from the system. Consequently, we have attempted to model phlogopite veinlet formation and peridotite metasomatism by allowing up to 10% phlogopite (in equilibrium with liquids between L_1 and L_2) and up to 30% of the residual liquid at L_2 to be incorporated into the adjacent peridotite, respectively (Fig. 4b). (It should be noted that the model developed here for alkaline magma generation in continental settings is valid only for regions where the lithosphere is no more than ~100 km thick; for thicker lithosphere the sequence and mode of fractionating phases is likely to be different from that used here.)

RESULTS

An example of a Monte Carlo simulation is described in the Electronic Appendix A (available at http://petrology.oxfordjournals.org/). We performed 30 000 such simulations by randomly varying the parameters listed in Figs 1, 2, and 4. Out of the 30 000 calculations, 1850 resulted in a negative Ti content in the most evolved liquids (L_2 in Fig. 4). This happens when high proportions of Ti-rich phases are removed from a melt produced by high degrees of melting (and thus having a relatively low initial TiO_2 content). Because, in nature, the appearance and modal proportions of the crystallizing Ti-rich phases will be strongly coupled with the Ti content of the melt, we have deleted those calculations in which the Ti content in the residual liquid (L_2 in Fig. 4) is less than half the primitive mantle concentration (i.e. <600 ppm Ti). What are shown in Fig. 5 are the results of 25 000 calculations randomly selected from the 25 733 calculations that produced Ti contents ≥600 ppm in L_2.

Figure 5a shows the trace-element compositions of DMM and E-DMM (Workman & Hart, 2005) that represent the range of our model asthenospheric peridotites, normalized to primitive mantle (PM; McDonough & Sun, 1995). Also shown are the calculated near-solidus melts (L_0; average, $\pm 1\sigma$, and maximum and minimum compositions) produced by 0·5–1·8 wt % melting (see Fig. 2b). These initial metasomatic liquids are enriched in incompatible trace elements relative to their source and to PM, show elevated La/Yb relative to PM, and have incompatible trace-element ratios (such as La/Nb, Ce/Pb, and Ba/Th) similar to the range observed in enriched MORB compiled by Salters & Stracke (2004). However, except for Pb, the average composition of the model L_0 liquids does not overlap with the field defined by basanitic lavas sampled at intraplate volcanoes (shown as a gray band; only the upper bound calculated for Rb, U, Th, and Pb partially overlaps with the lower portion of the basanite field); that is, these calculated liquids are insufficiently enriched in trace elements to match the observed concentrations in alkaline lavas from intraplate settings (Fig. 5a). Varying the degree of melting outside the 0·5–1·8 wt % range does change the trace-element abundances for the highly incompatible elements relative to the average partial melt composition plotted in Fig. 5a; however, both the relative and absolute concentrations of the moderately incompatible elements change little with the degree of melting. Thus, although the high concentrations of very incompatible elements such as Rb, Ba, U, and Th in basanites can be matched by near-solidus melts produced by degrees of partial melting lower than 0·5 wt %, such low-degree melts do not contain sufficient moderately incompatible trace-element contents (e.g. HREE) to match the abundances of these elements observed in basanites (see the $F = 0{\cdot}2$ wt % melt pattern in Fig. 5a). Thus, as described above for TiO_2 concentrations (Prytulak & Elliott, 2007), Fig. 5a shows that if basanites are to represent low-degree melts of lherzolites in the garnet-stability field, their sources must be enriched relative to E-DMM for all of the moderately incompatible trace elements.

The continuous lines labelled L_1 and L_2 in Fig. 5b show how the trace-element contents of the forward-modelled residual metasomatic liquids evolve with continued fractionation within the lithosphere. Liquid L_1 [average f (proportion of residual liquid) ~56%] reflects the composition after fractionation of clinopyroxene, olivine, and/or garnet ± orthopyroxene (the anhydrous cumulate assemblage) and just prior to the appearance of amphibole. Liquid L_2 (average f ~27%) reflects melt compositions following amphibole, clinopyroxene, minor garnet,

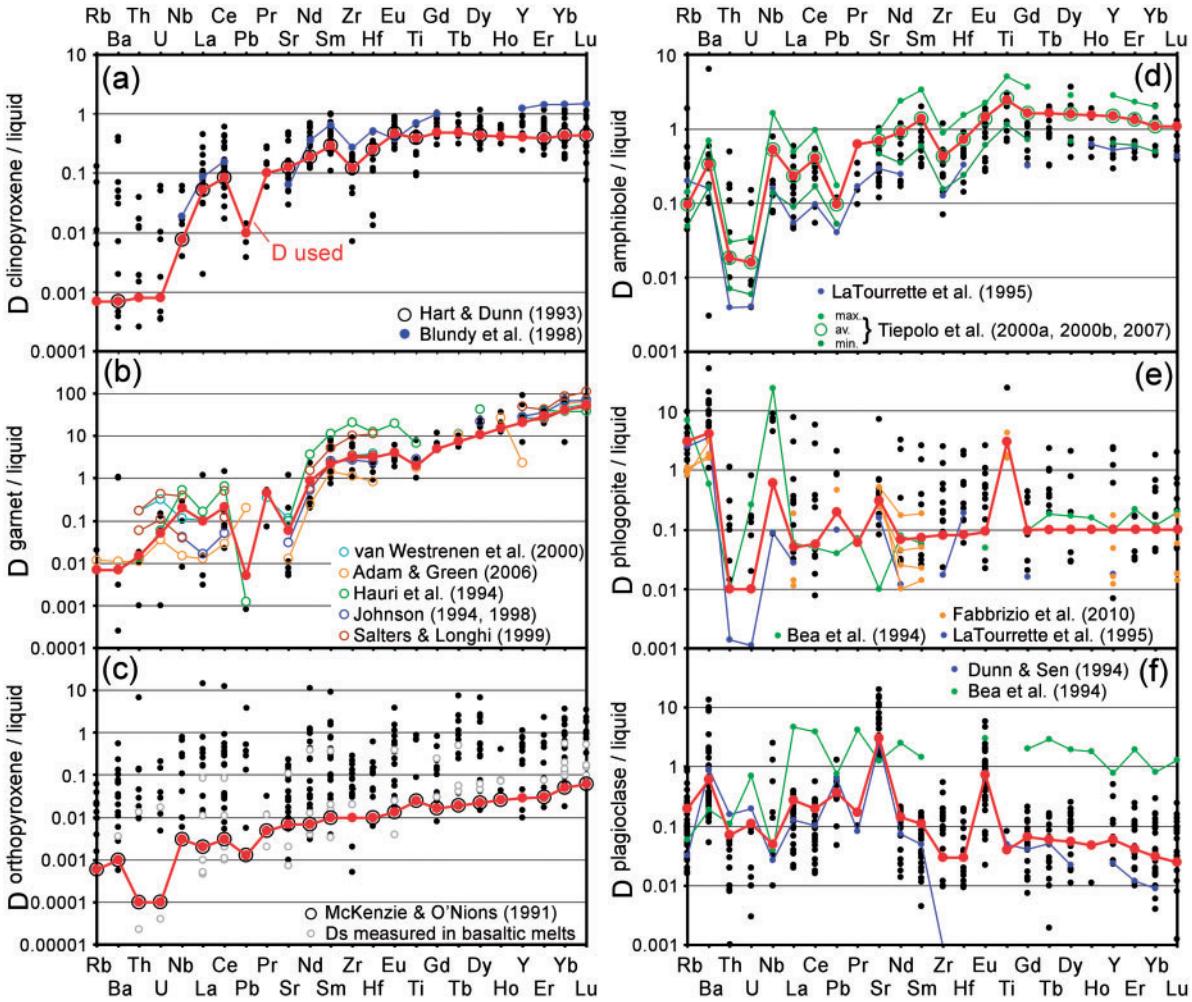

Fig. 3. Mineral/liquid partition coefficients ($D^{min/liq}$) from the literature for (a) clinopyroxene, (b) garnet, (c) orthopyroxene, (d) amphibole, (e) phlogopite, (f) plagioclase, (g) titanite, (h) ilmenite, (i) rutile, (j) apatite, (k) allanite, and (l) zircon. Large filled red circles show the values used in the Monte Carlo calculations in this study; smaller filled black circles and open gray circles are D values reported in the GERM partition coefficient database; references for the other colored circles are given in each panel. The pairs of D values in (b) associated with Salters & Longhi (1999) reflect minimum and maximum values, respectively. The values plotted as 'calculated Ds' for titanite, ilmenite, apatite, and allanite (g, h, j, and k) were determined in two steps. First, the accessory mineral (titanite, ilmenite, etc.)/amphibole D values were calculated using the trace-element compositions of these phases as measured by LA-ICP-MS in hydrous metasomatic veins from the French Pyrenees (both the accessory minerals and amphiboles were measured in the same rocks). Second, the $D^{min/liq}$ values for these accessory minerals were calculated by dividing $D^{min/amph}$ for each element by our preferred $D^{amph/liq}$ value (d) for that element.

orthopyroxene, phlogopite, plagioclase, and accessory phase crystallization. Although the concentrations of the most incompatible elements (e.g. Rb to Sr) are progressively enriched as liquids evolve from L_1 to L_2, neither pattern matches that of basanitic lavas from intraplate volcanoes. Although fractionation of garnet and clinopyroxene modify the LREE/HREE ratios of the evolving liquid compared with the initial metasomatic melt (compare L_0 to L_1 and L_2; Fig. 5b), nevertheless, the LREE/HREE ratios of L_1 largely reflect those of the initial near-solidus garnet-peridotite melt. Further, because the D values for olivine, clinopyroxene, and garnet for the trace elements considered in Fig. 5 are <1 (except for HREE in garnet; see Fig. 3a), the proportions of those phases that crystallize from L_0 do not significantly modify the trace-element ratios of the evolving liquid (i.e. the relative proportions of phases that crystallize from L_0 to L_1 are not critical parameters) and except for the increase in LREE/HREE ratios owing to garnet crystallization, the slope of the average L_1 pattern in Fig. 5b is grossly similar to that of the L_0 average.

Liquid L_2 is the end product of fractionation in our model, and it shows some specific differences from L_0 and L_1 (Fig. 5b). For example, liquid L_2 is characterized by

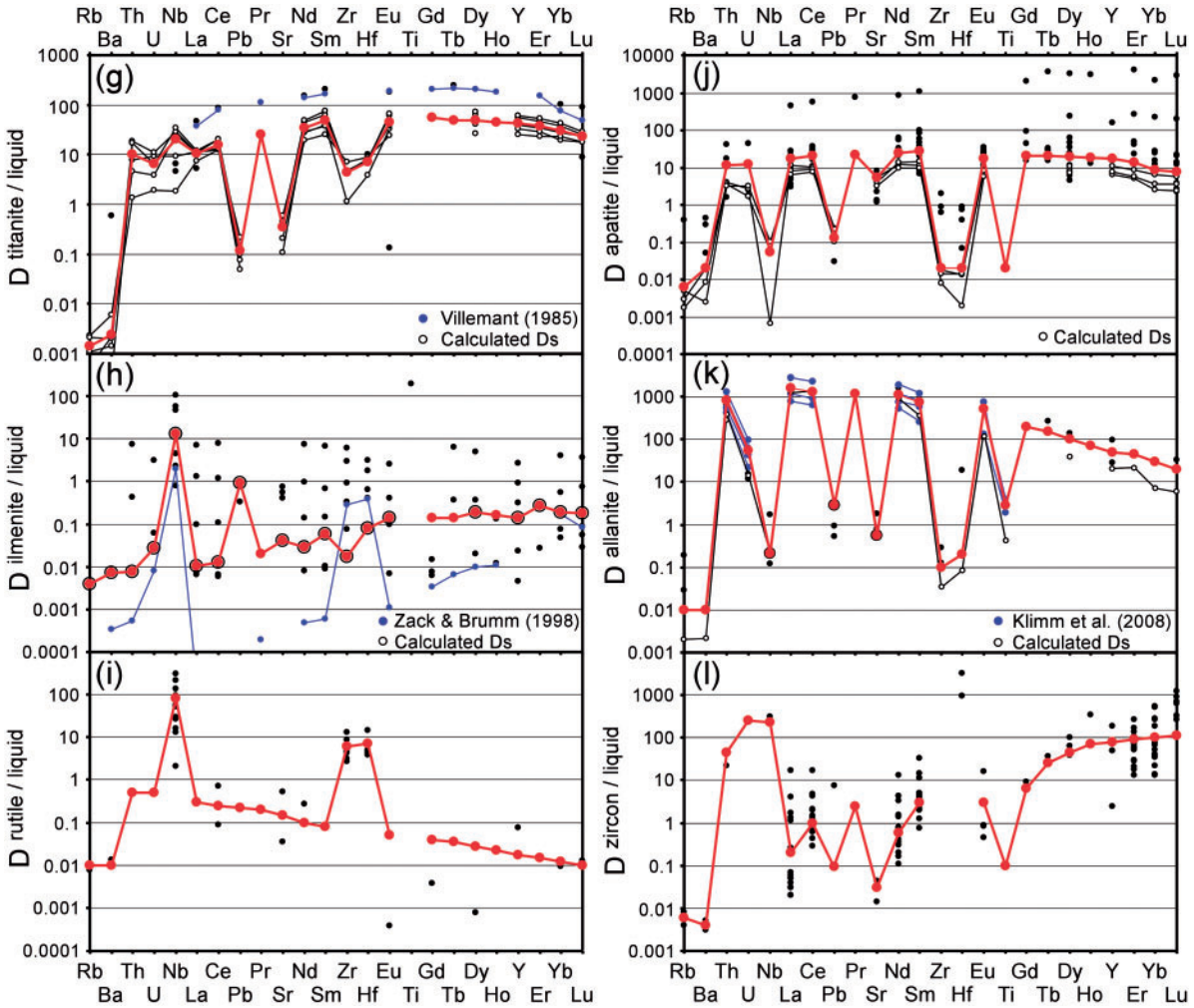

Fig. 3. Continued.

low Nb/La and Nb/Th ratios, reflecting the fractionation of amphibole and Fe–Ti oxides, phases that are enriched in Nb relative to La and Th (Fig. 3; Table 2). L_2 is also characterized by a distinct REE pattern compared with that of L_0 or L_1. L_2 shows a moderate depletion of middle REE (MREE) with respect to the LREE and HREE, a depletion that is not observed in liquid L_0 or L_1. Although the crystallization of amphibole can partially explain the relative decrease of the MREE with respect to the LREE and HREE in going from from L_1 to L_2 (amphibole/liquid *D* values are characterized by higher values for MREE than for the LREE or HREE; Fig. 3d), the main factor is the fractionation of titanite and apatite, minerals characterized by high mineral/liquid *D* values for all REE but with the highest values for the MREE (Fig. 3g and j). The fractionation of titanite, apatite, and allanite, minerals that incorporate the REE preferentially in comparison with Zr, Hf, Sr, and Pb (Fig. 3; Table 2), is also responsible for the development of positive anomalies for Zr, Hf, Sr, and Pb in the trace-element pattern of liquid L_2 (Fig. 5b).

Figure 5c shows the composition of the bulk model anhydrous cumulate assemblage (just prior to the appearance of amphibole) and the composition of the model hydrous cumulates. The trace-element patterns of the anhydrous cumulates (cpx + gt and/or ol ± opx) are depleted in highly incompatible elements such as Rb, Ba, U, and Th, have substantial negative Pb anomalies, and are relatively flat in the region of the REE (Fig. 5c). The variability in the concentrations of the most incompatible elements is primarily related to the presence of trapped liquid, which varies from 0 to 5%. The negative Pb and slightly negative Zr anomalies observed in the model anhydrous cumulates do not reflect the composition of the liquid from which these cumulates crystallized (L_0 does not show such negative anomalies; Fig. 5a)—these anomalies reflect the low

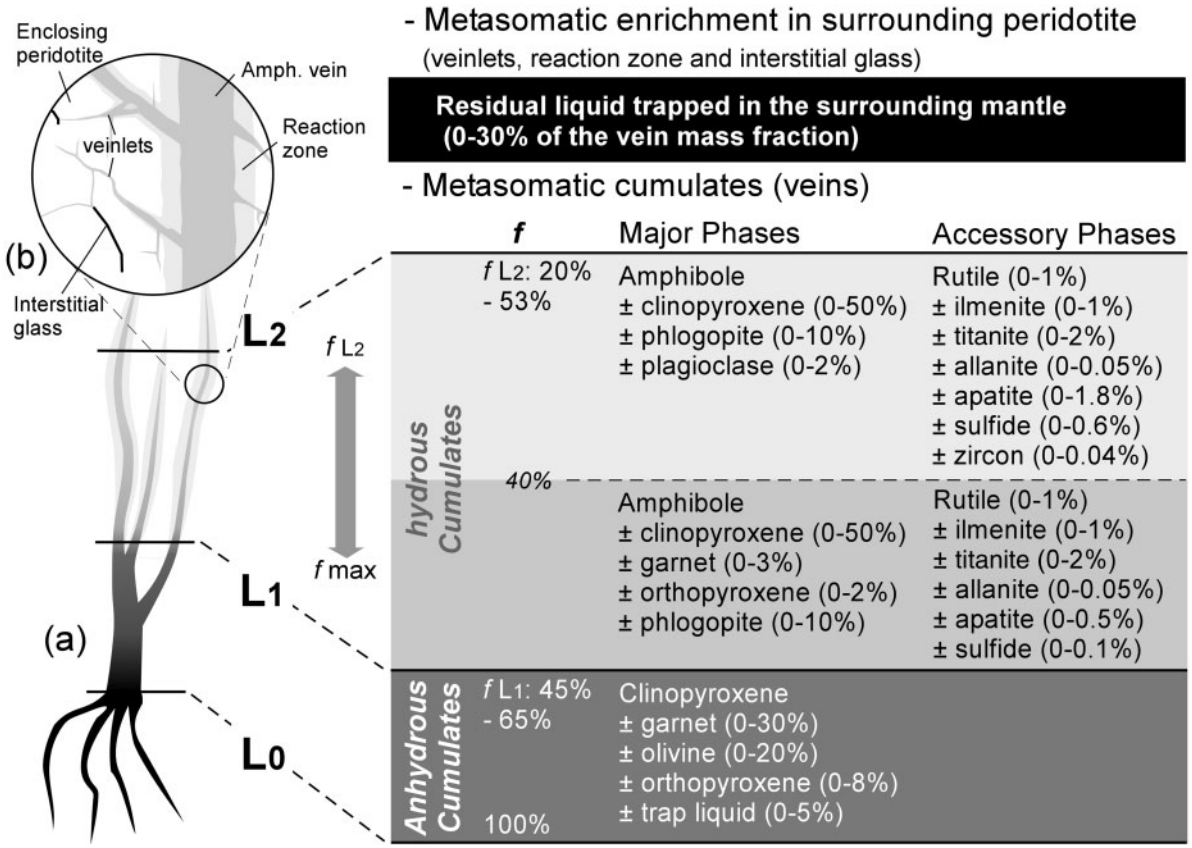

Fig. 4. (a) Phase proportions used in the Monte Carlo simulations. The percentages listed after each mineral show the bounds within which the proportions in the cumulate assemblage were free to vary; f is the proportion (in %) of residual liquid. The amount of residual liquid at the transition between anhydrous and hydrous cumulate formation (fL_1) is free to vary between 65 and 45%, whereas the amount of residual liquid (fL_2) at the end point of the calculation can vary from 53 to 20% (with the condition that $fL_2 < fL_1 - 10\%$). The compositions of hydrous cumulates are randomly calculated between $f$max ($< fL_1$) and fL_2 with the constraints that $fL_2 \geq 20\%$ and $f\text{max} - fL_2 > 10\%$. The proportion of clinopyroxene in the anhydrous cumulates and amphibole in the hydrous cumulates was calculated by difference (i.e. 100 − sum of all other phases). The proportion of garnet (gt) varied between 0 and 30% in the anhydrous cumulates; if the proportion of garnet was higher than 18% then no olivine (ol) crystallized; if the proportion of garnet was lower than 18% then olivine content was calculated using the formula % ol = rand(10–20) × [18 − (% gt)]/18, where rand(10–20) is a random number drawn from a flat distribution between 10 and 20. The sum of rutile + ilmenite (ilm) varied between 0 and 1%; rutile = rand(0–1); ilmenite was calculated using % ilm = rand(0–1) × [1 − (% rutile)]. The proportion of phlogopite (0–10%) in the veins represents the potential presence of veinlets in association with major metasomatic veins [see (b)]; the proportion of trapped liquid in the surrounding peridotite is linked to the proportion of phlogopite in the veins assuming that veinlets and metasomatism in the surrounding peridotite correspond to a unique process (the ratio of phlogopite to trapped liquid = 1:3). (See Electronic Appendix A for an example of the calculation.) (b) Schematic illustration of progressive infiltration of metasomatic melts within surrounding peridotite [modified from Fig. 1 of Wulff-Pedersen *et al.* (1999)].

$D^{\text{min/liq}}$ values for Pb and Zr in clinopyroxene and the low $D^{\text{min/liq}}$ for Pb in garnet relative to elements with similar degrees of incompatibility such as Ce and Pr for Pb and Sm and Eu for Zr (Fig. 3a and b). The variability of HREE contents in the anhydrous cumulates is directly related to the amount of cumulate garnet.

The model hydrous cumulates (amph and cpx plus minor opx, gt, phlog, pl, and accessory minerals) show distinctive trace-element patterns relative to the model anhydrous cumulates. These patterns are characterized by significantly higher concentrations of highly incompatible trace elements compared with the model anhydrous cumulates (Fig. 5c). For example, in the hydrous cumulates, the La content is ~2 to 85 times higher than the content calculated in the anhydrous cumulates. The high concentrations of incompatible elements in the model hydrous cumulates reflect (1) the relatively high $D^{\text{amph/liq}}$ values for most of these elements (exceptions are U, Th, and Pb), and (2) the presence of accessory minerals in the model hydrous cumulates such as apatite, allanite, titanite, and zircon, in which many of these trace elements reach very high concentrations. The model hydrous cumulates also have a positive Nb anomaly (i.e. elevated Nb/La relative to primitive mantle) owing to the high $D^{\text{amph/liq}}$ for

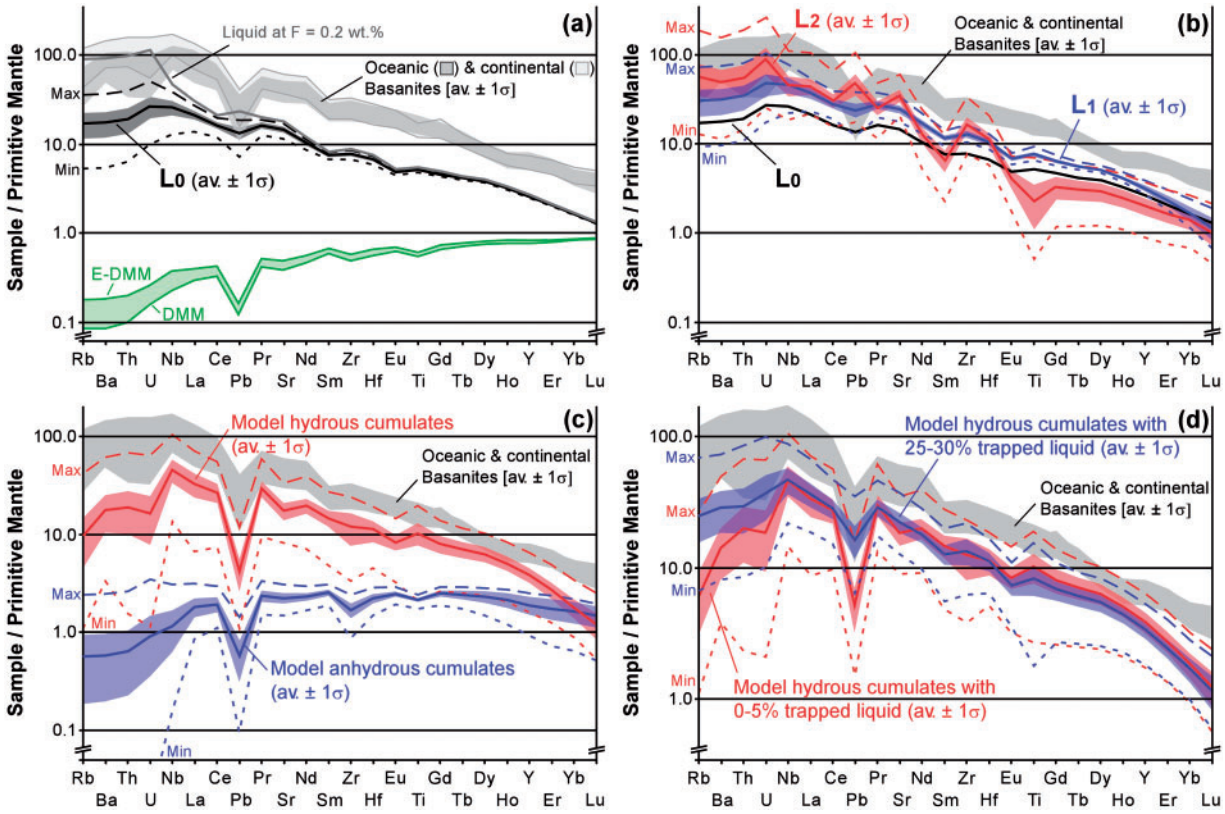

Fig. 5. (a) Trace-element contents (normalized to primitive mantle, PM; McDonough & Sun, 1995) of model-generated liquids produced by low-degree melting of the asthenosphere compared with continental and oceanic basanites and the assumed asthenospheric mantle end-members. L_0 is the composition of unfractionated H_2O and CO_2-bearing near-solidus peridotite melt; this composition corresponds to the initial melt entering the lithosphere from the underlying asthenosphere. The liquid labeled $F = 0{\cdot}2$ wt % represents a lower partial melting calculation and is discussed in the text. The green band corresponds to the compositional range of the asthenospheric mantle source used to generate L_0 (DMM to E-DMM; Workman & Hart, 2005). (b) Model-generated trace-element contents (normalized to PM) of the average L_0 [black curve from (a)], of residual liquids L_1 (blue) and L_2 (red) after fractionation of anhydrous and anhydrous + hydrous cumulates, respectively (see also Fig. 4b). (c) Model-generated trace-element contents (normalized to PM) of calculated anhydrous (blue) and hydrous (red) cumulates. (d) Model-generated trace-element contents (normalized to PM) of metasomatized hydrous lithosphere as function of the proportion of trapped liquid [0–5% (red) or 25–30% (blue)] in the surrounding peridotite. The composition of the metasomatized hydrous lithosphere ($C^{\text{met hyd lith}}$) is calculated using $C^{\text{met hyd lith}} = [100 - (\%\text{ trapped liq})] \times C^{\text{hyd cumulate}} + (\%\text{ trapped liq}) \times C^{\text{trapped liq}}$ where (% trapped liq) represents the proportion of trapped liquid (0–30%) in the peridotite surrounding the vein, $C^{\text{hyd cumulate}}$ represents the composition of the hydrous cumulates, and $C^{\text{trapped liq}}$ is the composition of the trapped liquid (i.e. liquid at fL_2). The dark-colored curves in each panel correspond to the average compositions of the liquids or cumulates, whereas the surrounding lighter-colored bands denote the $\pm 1\sigma$ range for the corresponding colored curves. The long and short dashed lines in each panel represent the maximum and minimum compositions, respectively, calculated in the simulations. The gray bands in (a)–(d) show the compositions of basanites from oceanic and continental intraplate volcanoes compiled from the GeoRoc database; for this compilation only basalts characterized by *ne*-normative compositions with SiO_2 contents between 40 and 45 wt % and with MgO contents between 8 and 15 wt % were selected. In (b)–(d), we do not distinguish between continental and oceanic basanites.

Nb relative to La and the presence of Fe–Ti oxides in the hydrous cumulates. Like the model anhydrous cumulates, the model hydrous cumulates also show a negative Pb anomaly with respect to the LREE, although it is even more negative than in the model anhydrous cumulates. This feature can be understood by the peculiarities of the partition coefficients of amphibole, titanite, apatite, and allanite (Fig. 3d, g, j, and k), although low $D^{\text{min/liq}}$ values for Pb relative to the LREE in clinopyroxene also contribute. The lower $D^{\text{min/liq}}$ values for Sr in comparison with LREE in titanite, apatite, and allanite (Fig. 3g, j, and k) also explain the small negative anomaly observed for Sr in the model hydrous cumulates.

None of the experimental studies that we used to constrain the crystallizing assemblages in our model produced significant phlogopite, and yet phlogopite is observed in cumulate veins and in smaller veinlets injected into the surrounding peridotite (Wilshire *et al.*, 1980; Bodinier *et al.*, 1990, 2004; McPherson *et al.*, 1996; Woodland *et al.*, 1996; Zanetti *et al.*, 1996; Wulff-Pedersen *et al.*, 1999; Moine *et al.*, 2001). In an effort to capture this feature of the natural hydrous veins and the surrounding metasomatized

mantle, we allowed up to 10% phlogopite as a crystallizing phase between L_1 and L_2. The presence of up to 10% phlogopite has a limited effect on the trace-element contents of the model metasomatic veins since phlogopite/liquid D values are <1 for most of the elements in Fig. 5 (see Fig. 3e). Only the concentrations of Rb and Ba (and to a lesser extent Ti and Nb) in the hydrous cumulates (Fig. 5c) are modified by the presence of phlogopite (of all the phases that make up the hydrous cumulate assemblage, phlogopite has the highest Rb and Ba partition coefficients). Finally, we modelled the presence of glass selvages and interstitial 'glass pockets' within the peridotite that surrounds the amphibole-bearing metasomatic veins by including a trapped liquid component (L_2) along with the hydrous cumulate assemblage. Although the proportion of trapped liquid is difficult at best to constrain, we have limited its proportion to be no more than 30%. Here and in the remainder of the discusion, we use the term 'metasomatized hydrous lithosphere' to describe the following packet of materials: hydrous cumulates (i.e. the vein assemblage) with 0–10% phlogopite and 0–30% trapped liquid (i.e. the associated metasomatized mantle). Comparing the trace-element pattern of model hydrous cumulates (Fig. 5c) with that of the hydrous cumulates plus various proportions of trapped liquid (0–5% or 25–30%; Fig. 5d) indicates that neither the slope of the REE nor the overall trace-element pattern of the hydrous cumulates is substantially modified by the addition of the trapped liquid that we use to mimic metasomatism in the mantle peridotite bordering the hydrous veins. Nevertheless, abundances of the very incompatible elements such as Rb, Ba, U, Th, Pb, and Sr are sensitive to the proportion of trapped melt (Fig. 5d). In particular, the Nb/U, Nb/Th, and Ce/Pb ratios of the metasomatized hydrous lithosphere decrease significantly with the progressive addition of trapped liquid, whereas the Sr/Nd ratio shows the opposite behaviour. These effects reflect the specific trace-element pattern of liquid L_2 (Fig. 5b) with respect to the composition of the hydrous cumulates (Fig. 5c).

DISCUSSION

Comparison of natural and model amphibole compositions

A critical goal of this study was to evaluate the composition of hydrous cumulates produced by fractional crystallization of low-degree melts of the asthenosphere as they pass through the lithosphere—cumulates that are interpreted as a major component of the sources of alkaline intraplate magmas (Halliday *et al.*, 1995; Niu & O'Hara, 2003; Pilet *et al.*, 2004, 2005, 2008). Before evaluating the key geochemical characteristics of the model hydrous cumulates and related partial melts to those of natural alkaline lavas, we first compare amphibole compositions predicted by the model with the compositions of amphibole observed in metasomatic veins worldwide. Figure 6 shows that model amphibole compositions are similar to the natural amphiboles and that the model amphiboles reproduce critical aspects of the trace-element patterns of amphiboles from oceanic and continental metasomatic veins. In particular, both the model and natural amphiboles are characterized by significantly elevated Nb/La ratios relative to primitive mantle; by low U and Th contents relative to elements of similar compatibility [with the exception of amphiboles from Kergelen xenoliths (Moine *et al.*, 2001), which do not show these low U and Th contents]; by negative Pb anomalies relative to LREE of similar compatibility; and by having similar REE slopes. The high Nb/La and low Nb/U and Ce/Pb ratios in the model amphiboles reflect the specific $D^{amph/liq}$ values for these elements (Fig. 3d; Table 2) rather than the composition of the liquids from which these amphiboles crystallized [liquids L_1 and L_2 (Fig. 5b) do not show these anomalies]. The overall similarity between the two sets of patterns suggests that our model for the origin of amphibole-rich veins in the lithosphere is on the right track. The calculated amphiboles do differ from those observed in metasomatic veins in that they have lower overall trace-element contents (Fig. 6); for example, the average La concentration (in ppm) in amphiboles from metasomatic veins is 39 ± 30 (1σ) whereas the average for the model amphiboles is $10{\cdot}6 \pm 3{\cdot}1$ (1σ). These differences in trace-element abundances may reflect several factors. The initial melt (L_0) could be insufficiently enriched in trace elements relative to the actual parental melts of the metasomatic vein cumulates; either lowering the degree of melting (assumed to be 0·75 on average) or postulating sources more enriched than the E-DMM composition of Workman & Hart (2005), the upper limit in our model source, would elevate the calculated amphibole patterns without altering their shapes. Alternatively, the amphibole/liquid D values that we use may be systemically low. Tiepolo *et al.* (2000*a*, 2000*b*) showed that REE, Y, Nb, U, and Th amphibole/liquid D values increase by factors of 3–7 for most elements with increasing melt polymerization ($D^{amph/liq}$ for Nb seems, in particular, highly affected by this melt compositional control, with D increasing from 0·13 for liquids with ~43 wt % SiO_2 to D vaslues ranging from 0·5 to 1·6 for liquids with ~55 wt % SiO_2). Because we cannot at present calculate the major-element composition of the evolving liquid, we have simply averaged the experimental amphibole/liquid D values (Tiepolo *et al.*, 2000*a*, 2000*b*). Ti contents of the model amphiboles are also low relative to Ti concentrations measured in natural amphiboles from metasomatic veins. However, Pilet *et al.* (2010) have shown that $D^{amph/liq}$ for Ti correlates with crystallization

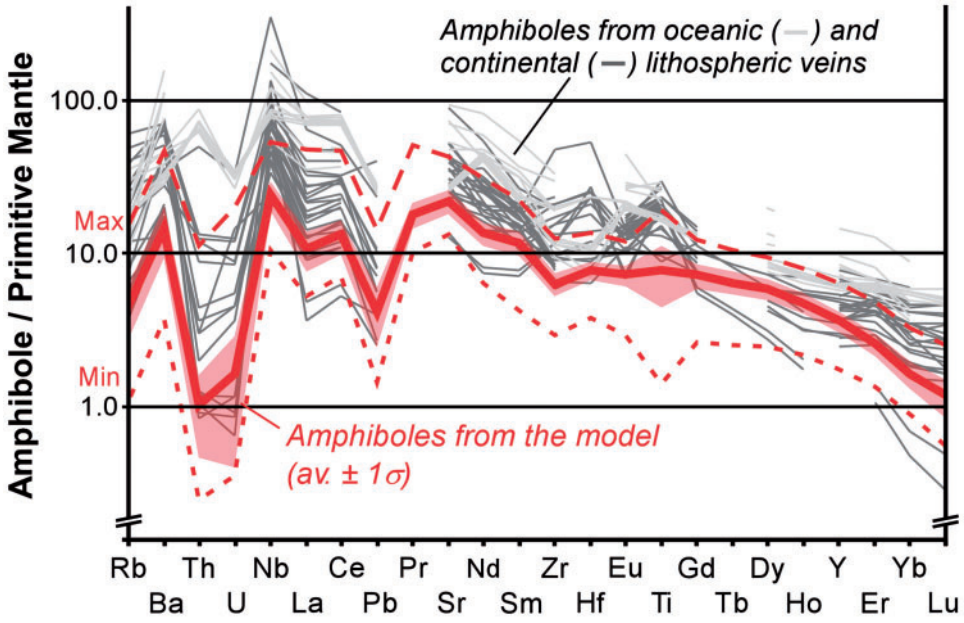

Fig. 6. Trace-element contents (normalized to PM; McDonough & Sun, 1995) of amphiboles from the model hydrous cumulates (dark red curve) compared with amphibole compositions from metasomatic veins observed in oceanic (light gray) and continental (dark gray) settings (Ionov & Hofmann, 1995; Vaselli *et al.*, 1995; Zanetti *et al.*, 1996; Wulff-Pedersen *et al.*, 1999; Moine *et al.*, 2001; Downes *et al.*, 2004; Pilet *et al.*, 2008). For the model calculations, the light red band shows the $\pm 1\sigma$ variation; the long and short red dashed lines represent maximum and minimum values from the calculations, respectively.

temperature and structure of the coexisting silicate melt (over a temperature interval from 1130 to 950°C, amphibole/liquid D_{Ti} could vary from ~2 to ~6). Therefore, we assume that the discrepancy in Ti contents between the model and the natural amphiboles (Fig. 6) reflects our choice of a constant $D^{amph/liq}$ for Ti (2·5; Table 2). For these reasons, we consider the match between the overall shapes of the calculated and observed trace-element patterns and the presence of certain diagnostic positive (e.g. Nb) and negative (e.g. Th, U, and Pb) anomalies to be more significant tests of the model than reproducing the absolute concentrations.

Comparison of natural alkaline magmas and model melts of metasomatized hydrous lithosphere

The model low-degree partial melts of typical depleted asthenospheric mantle (or the differentiated liquids of these partial melts) are a poor compositional match in terms of trace and minor elements to alkaline magmas from ocean islands and continental massifs (i.e. estimates of L_0 do not match the gray fields labelled 'basanites' in Fig. 5a). This confirms that such melts, widespread on the continents and in the ocean basins, require some other mode of origin (Gast *et al.*, 1964; Hart, 1988). Our focus in this and previous studies (Pilet *et al.*, 2005, 2008) has been to develop and test the hypothesis that melting of metasomatized lithosphere can explain the geochemical featuers of these alkaline magmas, but we emphasize that there are several alternatives, including the possibility of melts of metasomatized peridotites with source compositions different from typical mantle (Sun & McDonough, 1989; McKenzie & O'Nions, 1995); melts of mixtures of peridotite and other components (Chase, 1981; Hofmann & White, 1982); and/or the involvement of components with complex compositional characteristics reflecting processes occurring in subduction zones and elsewhere in the mantle (Weaver, 1991; Chauvel *et al.*, 1992; Panter *et al.*, 2006; Willbold & Stracke, 2006; Elliott *et al.*, 2007). Our goal here is not to explore the pros and cons of these various alternatives, but rather to evaluate the viability and consequences of the metasomatized lithosphere model. Pilet *et al.* (2008) demonstrated that high-degree partial melts of naturally occurring hydrous veins in metasomatized lithosphere overlap compositionally with alkaline magmas and thus that they can indeed plausibly represent significant components of the sources of such magmas. The models presented here explore the mechanisms by which such hydrous veins might have formed, and in this section we employ these models of cumulate formation to examine the origin of particular geochemical features in such rocks and how they might connect to the features observed in alkaline magmas.

The calculated anhydrous cumulate compositions shown in Fig. 5c indicate that such cumulates can exhibit

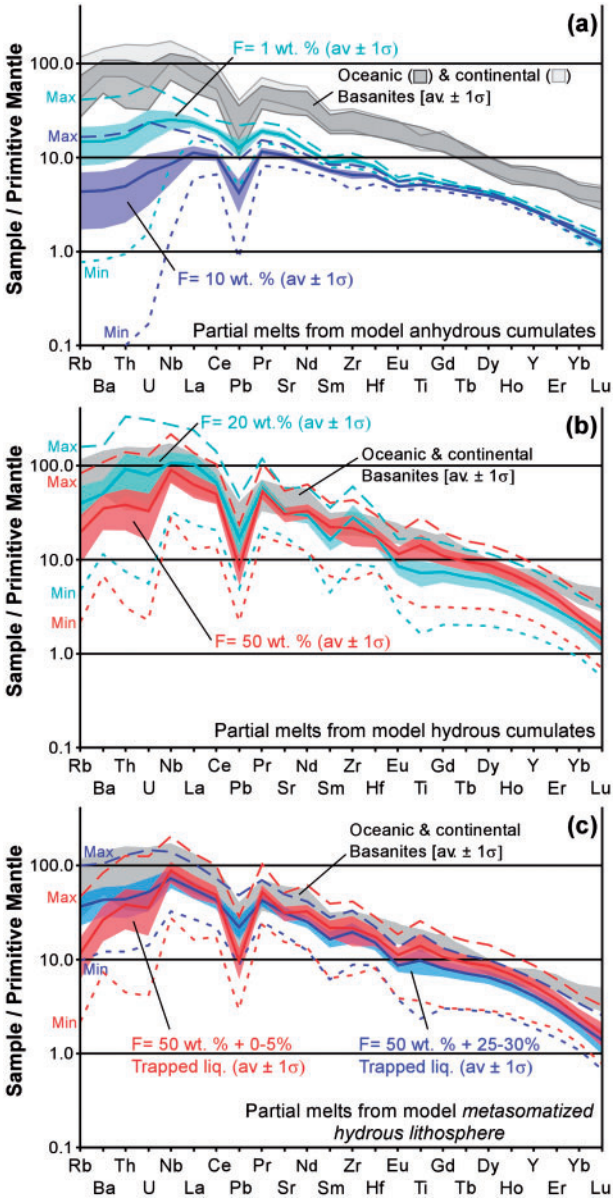

Fig. 7. (a) Model generated trace-element contents (normalized to PM; McDonough & Sun, 1995) of melts produced by 1 wt % (cyan) and 10 wt % (blue) partial melting of the model anhydrous cumulates compared with oceanic and continental basanites (see Fig. 5 caption). The trace-element contents were calculated assuming modal batch melting, mineral modes from model anhydrous cumulates, and D values reported in Table 2. (b) Trace-element contents (normalized to PM) of melts produced by 20 wt % (cyan) and 50 wt % (red) partial melting of the model hydrous cumulates compared with oceanic and continental basanites. The bands define trace-element contents calculated using the incongruent melting reaction for amphibole at 1·5 GPa [Pilet *et al.* (2008), 1 amph → 0·6 liq + 0·3 cpx + 0·1 ol], mineral modes from the model hydrous cumulates, and D values reported in Table 2. We also assumed that all accessory minerals (phlogopite, titanite, apatite, ilmenite, rutile, allanite, and zircon) are completely melted by 20 wt % melting. (c) Comparison of trace-element contents of oceanic and continental basanites (normalized to PM) with those of melts produced from metasomatized hydrous lithosphere composed of hydrous veins plus 0–5% (red) or 25–30% (blue) trapped liquid (L_2) simulating metasomatism of the surrounding peridotite (see text and Fig. 5 caption). The composition of the liquid from the hydrous cumulates is calculated at 50 wt % melting [see (b)]; the contribution from the metasomatized peridotite is calculated by assuming that all elements added by the metasomatic process are removed from the surrounding peridotite during the melting of metasomatized hydrous lithosphere [in practice, this corresponds to adding various fractions of liquid L_2 (Fig. 5b) to the composition of the hydrous cumulate melts]. The dark-colored curves in each panel show the calculated average compositions of the partial melts whereas the surrounding lighter-colored bands indicate the corresponding $\pm 1\sigma$ variation. The long and short dashed lines associated with each of the colored bands represent the maximum and minimum compositions calculated in the simulations. The gray bands in (a)–(c) show the compositions of basanites from oceanic and continental intraplate volcanoes [in (b) and (c), we do not distinguish between continental and oceanic basanites].

significantly different trace-element concentrations and patterns depending on their garnet to olivine ratio and on the proportion of trapped liquid. However, neither the composition of such cumulates nor their calculated low-degree partial melts overlap the compositions of oceanic or continental basanites (Fig. 7a). These cumulates are thus unlikely to contribute significantly to the trace-element budget of alkaline magmas, especially as such lithologies entrained in an upwelling mantle plume would be expected to melt to a large degree (Hirschmann & Stolper, 1996; Ito & Mahoney, 2005*a*; Stolper & Asimow, 2007), such that melts of such rocks would not differ significantly overall from the sources themselves.

In contrast to the model anhydrous cumulates, the model hydrous cumulates and metasomatized hydrous lithosphere (hydrous cumulates plus trapped residual liquids) have trace-element patterns that are similar to the average pattern observed in basanites from oceanic islands and from intracontinental volcanoes (Fig. 5c and d), although the model cumulate compositions are about a factor of ~2–6 lower than the actual lavas. Also shown in Fig. 7b are calculated trace-element patterns for 20 and 50 wt % partial melts of the range of hydrous cumulates shown in Fig. 5c based on their model modal abundances, mineral/liquid D values reported in Table 2, and melting reaction for hornblendite (±cpx) at 1·5 GPa from Pilet *et al.* (2008). The compositional range of the liquids produced by 20 wt % melting of the model hydrous cumulates (from Min to Max; Fig. 7b) overlaps the composition of basanites observed in continental or oceanic settings. However, the trace-element patterns of these melts differ in some details from natural basanitic lavas. For example, the model 20 wt % partial melts show concave-down REE patterns and positive Zr and Hf anomalies with respect to the MREE whereas the natural basanites do not show these features. These positive Zr and Hf anomalies with respect to the MREE are consistent with the presence of significant residual amphibole in the model source; that

is, amphiboles have mineral/liquid D values for MREE to HREE >1 whereas Zr and Hf are incompatible ($D^{amph/liq}$ <1; Fig. 3d). In contrast, liquids produced by 50 wt % partial melting of the hydrous cumulates show trace-element patterns that are overall very similar to those of oceanic or continental basanites (Fig. 7b), although they have slightly lower concentrations than the natural basanites. The difference between these two trace-element patterns reflects the loss of amphibole between 20 and 50 wt % melting in our models.

As indicated above, it is important to consider the potential contribution of the metasomatized peridotite surrounding the hydrous cumulates as this material will also have a low solidus temperature relative to unmetasomatized peridotite and thus could potentially melt during upwelling or heating and contribute to the trace-element inventories of melts of metasomatized lithosphere. Figure 7c shows the composition of melts from metasomatized hydrous lithosphere (equal to hydrous cumulates plus trapped liquid, L_2; see discussion above). In this calculation, we assumed that the hydrous veins melt to 50 wt % and that all trace elements associated with the trapped liquid (the mantle metasomatic component) are added to these 50 wt % partial melts. This approach is supported by the observation that, for metasomatized peridotites, incompatible trace elements are not incorporated within the major mineral phases (e.g. ol, opx, cpx, and spinel), but are localized in melt inclusions, pervasive grain-boundary components, or interstitial minerals (Bedini & Bodinier, 1999). As with the 50% melts of the hydrous veins (Fig. 7b), the melts from metasomatized hydrous lithosphere display a good match with the trace-element patterns of oceanic and continental basanites (Fig. 7c). The variations in melt composition as a function of the fraction of the metasomatized peridotite component are in general not large, but can be significant with respect to highly incompatible elements such as Rb, Ba, and Pb and related ratios such as Rb/Sr, Ba/Nb, and Ce/Pb (Fig. 7c).

The high-degree partial melts of the model hydrous cumulates, with or without a contribution from metasomatized peridotite, match well the observed range of natural basanitic magmas from ocean islands and from the continents (Fig. 7b and c), supporting the hypothesis that metasomatic veins in the lithosphere play a significant role as sources of these widespread mantle-derived magmas. It should be noted that although the most enriched model liquids (dashed lines denoted as Max in Fig. 7b and c) generally overlap with the most enriched basanite compositions, the average model liquids have trace-element contents that are somewhat depleted relative to the concentration levels observed in most basanites. As in the case with the small but systematic mismatch between the trace-element contents of the model amphiboles and the natural amphiboles (see Fig. 6), this difference in trace-element contents between the model liquids and the natural basanites may reflect either small but systematic errors in the amphibole/liquid D values we used, or in our use of a DMM to E-DMM source that is slightly more depleted than the actual source of the initial low-degree peridotite partial melts.

Figure 8 compares several trace-element ratios in the model metasomatic liquids (L_0, L_1, and L_2), in the model hydrous cumulates, and in the calculated partial melts from the model metasomatized hydrous lithosphere (hydrous cumulates plus up to 30% trapped liquid) with the same ratios in primitive continental and oceanic intraplate alkaline basalts (i.e. in basalts characterized by *ne*-normative compositions and by MgO contents between 6 and 20 wt %). Rb/Sr, Sm/Nd, U/Pb, Ba/Nb, Ce/Pb, and Nb/U ratios were selected because they are used to characterize OIB sources as being representative of HIMU or EM sub-types (Hofmann & White, 1982; Hofmann *et al.*, 1986; Sun & McDonough, 1989; Weaver, 1991; Chauvel *et al.*, 1992; Halliday *et al.*, 1995; Willbold & Stracke, 2006). Figure 8g–l shows that the ranges of trace-element ratios calculated for the melts from metasomatized hydrous lithosphere reproduce most of the variability observed in primitive alkaline lavas shown in Fig. 8m–r (a subset of these lavas are plotted in Fig. 8s–x and are designated as HIMU, EM, or 'normal' on the basis of their isotopic compositions). Only for Ba/Nb ratios do the calculated melts show a range slightly lower than that observed in natural alkaline basalts. The model liquids also reproduce the variability seen in ratios that we have not plotted in Fig. 8, such as Nb/La and La/Yb. The variability in Sm/Nd, U/Pb, Ce/Pb, and Nb/U ratios in the calculated melts shown in Fig. 8h, i, k, and l is only weakly related to the compositional variability of the initial metasomatic melt (L_0 in Figs 4, 5, and 8b, c, e, and f); it is largely controlled by crystal–liquid fractionation and by the proportion of trapped liquid (Fig. 8h, i, k, and l). Figure 8a–f shows that the source variability (DMM to E-DMM) and variability in the degree of partial melting (0·5–1·8%) produces liquids (L_0) with relatively constant trace-element ratios. The exceptions are Rb/Sr and Ba/Nb where significant variations in these two ratios can be produced by varying the degree of partial melting of an asthenospheric source. The overall similarity in the values of the depicted trace-element ratios in L_0 and L_1 (Fig. 8a–f) reflects that fractionation of clinopyroxene ± garnet ± olivine is not efficient in significantly fractionating incompatible trace elements (with the exception of HREE, which are compatible in garnet). On the other hand, the fractionation of amphibole and accessory minerals significantly modifies most of the trace-element ratios of L_2 relative to L_1 and thereby introduces substantially more variability. The proportions of amphibole, ilmenite, rutile, and titanite also exert a

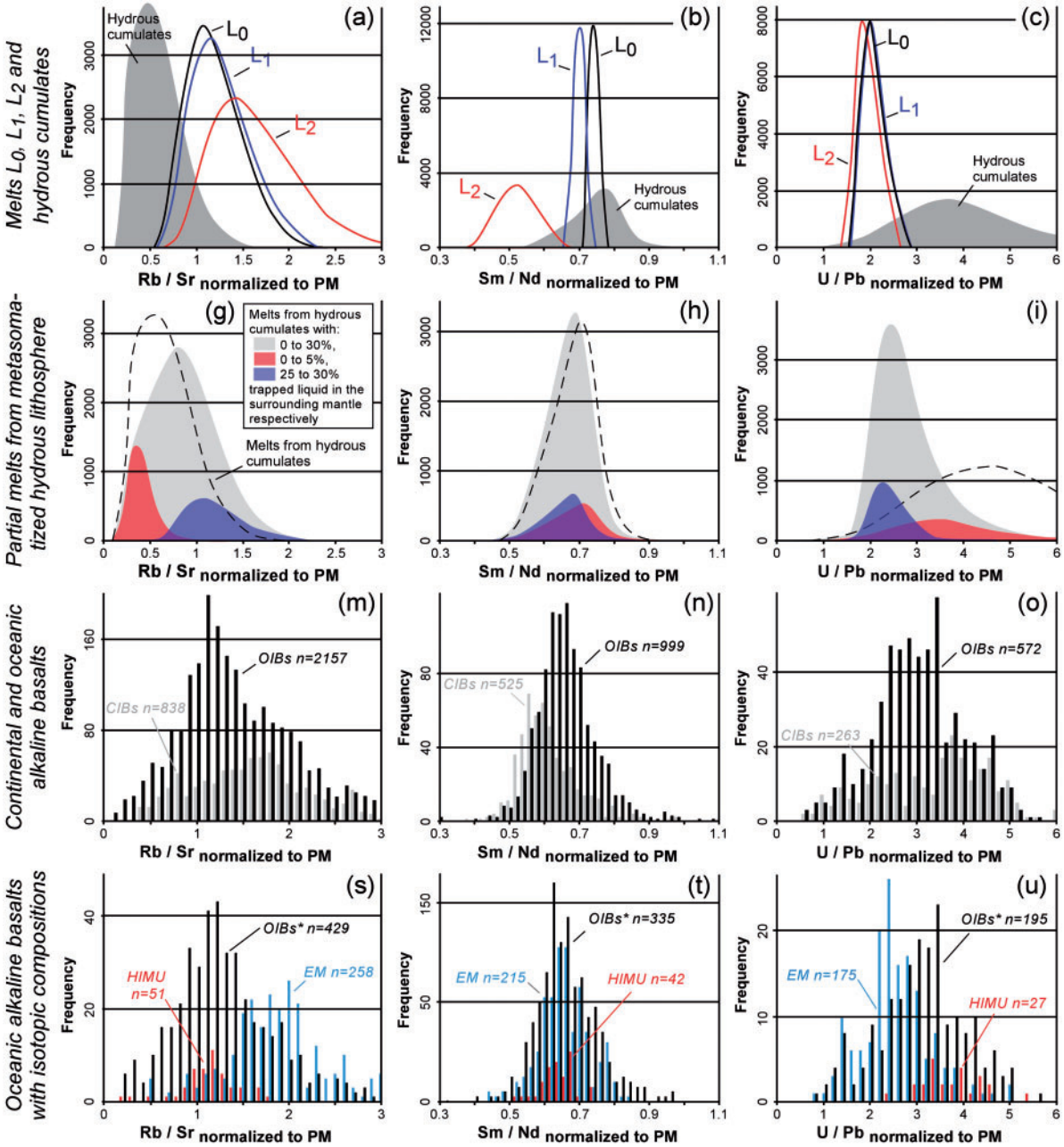

Fig. 8. (a–f) Distributions of trace-element ratios (a, Rb/Sr; b, Sm/Nd; c, U/Pb; d, Ba/Nb; e, Ce/Pb; f, Nb/U; all normalized to PM, McDonough & Sun, 1995) in calculated liquids L_0, L_1, L_2, and in the hydrous cumulates. (g–l) Distributions of PM-normalized trace-element ratios (g, Rb/Sr; h, Sm/Nd; i, U/Pb; j, Ba/Nb; k, Ce/Pb; l, Nb/U) in the model hydrous cumulates (dashed line) and in 50% partial melts of metasomatized hydrous lithosphere containing 0–5% (red area), 0–30% (gray area), and 25–30% (blue area) trapped liquid in the surrounding peridotite. (m–r) Distributions of PM-normalized trace-element ratios (m, Rb/Sr; n, Sm/Nd; o, U/Pb; p, Ba/Nb; q, Ce/Pb; r, Nb/U) in alkaline OIB (black lines) and alkaline continental intraplate basalts (CIB; gray lines) selected from the GeoRoc database. All basalts shown in (m)–(x) have normative nepheline, MgO contents between 6 and 20 wt %, and for continental lavas, K_2O/Na_2O weight ratios <1. (s–x) Distributions of PM-normalized trace-element ratios (s, Rb/Sr; t, Sm/Nd; u, U/Pb; v, Ba/Nb; w, Ce/Pb; x, Nb/U) in alkaline OIB with published Sr, Nd, and Pb isotopic compositions. These OIB data are labelled as HIMU if their $^{206}Pb/^{204}Pb$ ratio is higher than 20·3 (red); as EM if their $^{143}Nd/^{144}Nd$ or $^{87}Sr/^{86}Sr$ isotopic composition is lower than 0·51275 or higher than 0·704, respectively (blue); or 'normal' OIB (OIB*; black); these 'normal' compositions are plotted as small gray circles in Fig. 9a and c.

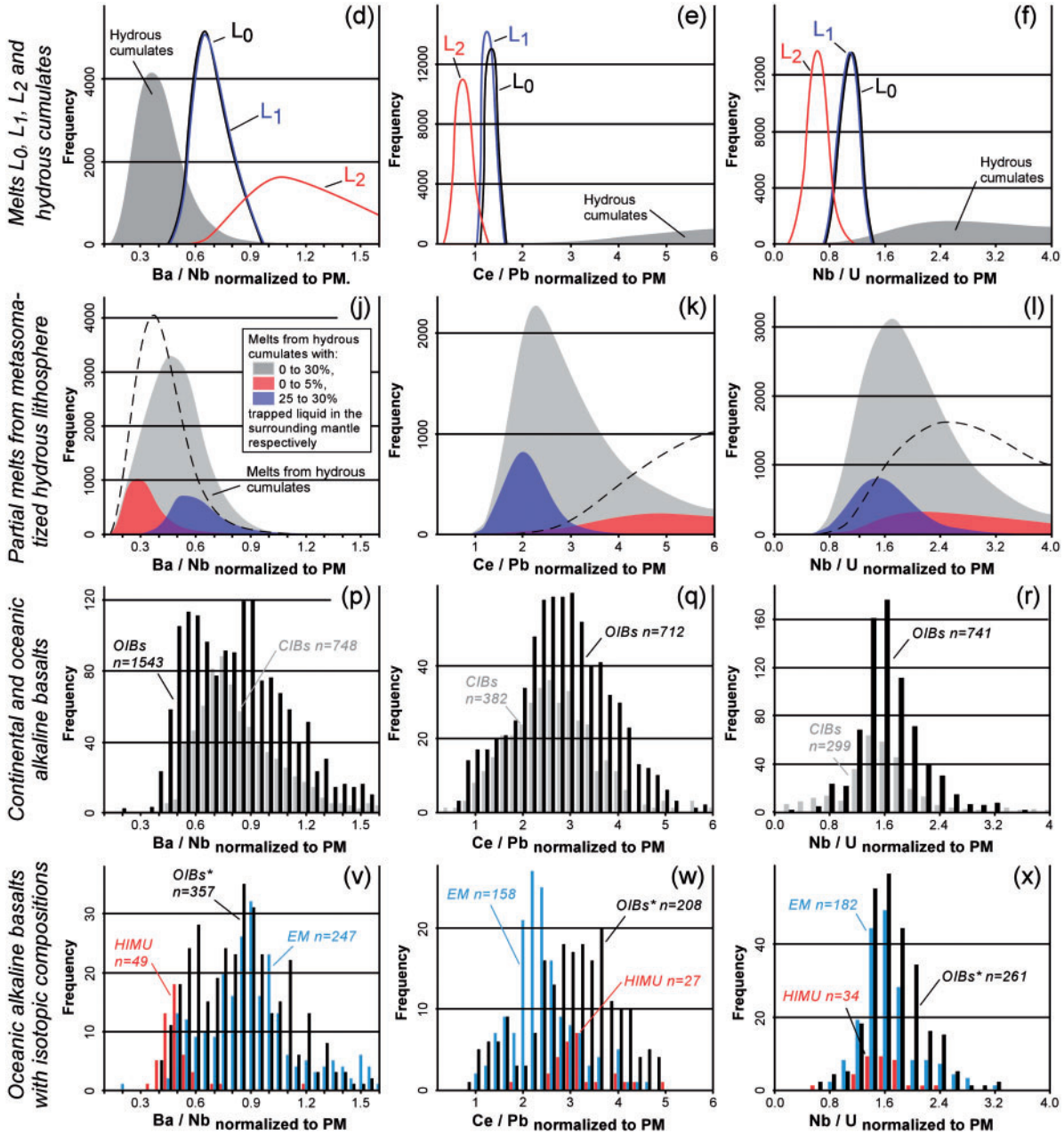

Fig. 8. Continued.

significant influence over the Ba/Nb and Nb/U ratios by preferentially fractionating Nb relative to Ba and U. The REE concentrations in the hydrous cumulates are highly correlated with the amount of titanite, apatite, and allanite that are present, whereas the proportion of sulfide, the only Pb-compatible phase in the model cumulates, influences the U/Pb and Ce/Pb ratios.

The variability of trace-element ratios in OIB and intracontinental basalts (Fig. 8m–r) is most often interpreted as due to the existence of several distinct end-members in the mantle sources of these basalts (Hart, 1988; Nakamura & Tatsumoto, 1988; Weaver, 1991; Chauvel *et al.*, 1992; Dixon *et al.*, 2002; Stracke *et al.*, 2003; Willbold & Stracke, 2006; Stracke & Bourdon, 2009). The trace-element ratio variability generated by our Monte Carlo modelling is consistent with the alternative hypothesis proposed by Pilet *et al.* (2005)—that the variability of trace elements observed in alkaline lavas of

continental and oceanic settings can be linked to variations in the compositions of metasomatic veins present in their sources. Figure 8g–l also indicates that, in addition to variations in the composition of metasomatic veins, another important parameter in the context of our model is the amount of cryptic and modal metasomatism associated with the veins; in particular, significant amounts (up to 30%) of such components are required in our model to explain the observed distributions of U/Pb, Ce/Pb, and Nb/U ratios of continental and oceanic alkaline magmas (compare Fig. 8i, k, and j with Fig. 8o, q, and r, respectively). The results of our model calculations suggest, therefore, that metasomatized hydrous lithosphere (hydrous veins + metasomatism in the surrounding mantle) produced by the differentiation of low-degree melts from a source similar to that of MORB can for the most part satisfy the observed trace-element contents (Fig. 7c) and associated ratios (Fig. 8) in alkaline magmas.

Isotopic evolution of metasomatized hydrous lithosphere over time

As indicated above, two scenarios have been proposed for the production of alkaline magmas by melting of metasomatized lithosphere (Halliday *et al.*, 1995; Niu & O'Hara, 2003; Pilet *et al.*, 2005, 2008): (1) shortly after or coincident with metasomatism, the lithosphere experiences a thermal perturbation or decompression and thereby melts *in situ*; or (2) the metasomatized lithosphere is recycled into the convecting mantle by subduction or delamination and melts during later upwelling (e.g. in a plume or at a ridge). Given the highly variable parent–daughter ratios of the major radiogenic isotope systems (e.g. Rb/Sr, Sm/Nd, and U/Pb) predicted for metasomatized hydrous lithosphere (Fig. 8g–i; ratios in the partial melts are approximately equal to those in the source), the metasomatized lithosphere model makes specific predictions about the temporal evolution of radiogenic isotope ratios depending on the mineralogy of the veins, the amount of trapped liquid in the surrounding peridotite, and the time interval between vein formation and melting. In this section, we explore how the isotopic compositions of the hydrous cumulates plus trapped liquid will evolve as a function of time and compare these evolving ratios with the observed isotopic compositions of mantle-derived alkaline magmas.

Figure 9 (a-I to a-IV) compares the isotopic compositions of OIB with the calculated compositions of metasomatized hydrous lithosphere assuming that this lithosphere was formed 0.15 Gyr ago. An age of 0·15 Ga corresponds to that of the oldest oceanic lithosphere observed on the Earth and thus potentially represents the longest isolation time for the *in situ* melting hypothesis for the generation of alkaline basalts in an oceanic setting. The ranges in Sr, Nd, and Pb isotopic compositions for this 0·15 Ga metasomatized lithosphere were calculated in two steps, as follows. (1) We calculated the isotopic composition of depleted MORB mantle (DMM to E-DMM) 0·15 Gyr ago assuming that the isotopic compositional range of these two MORB mantle end-members was similar to the range of isotopic compositions observed in MORB today and that they were formed by an instantaneous depletion event at 2·5 Ga. (2) The isotopic evolution of the metasomatized lithosphere from 0·15 Ga to the present was calculated using the Rb/Sr, Sm/Nd, and U/Pb ratios calculated for each of the 25 000 Monte Carlo simulations; these present-day values are shown as light gray, blue, and red points in the panels in Fig. 9a-I to a-IV (an example of this calculation as well as the various parameters that we used is presented in Electronic Appendix B). We assume that there is no diffusive interaction between metasomatized and unmetasomatized lithosphere, an assumption that is supported by the relatively low temperatures in the lithosphere and the relatively short time scale of this calculation.

The range of isotopic compositions calculated for a metasomatized lithosphere isolated for 0·15 Gyr is significantly larger than the compositions exhibited by MORB (which is taken as a proxy for the isotopic composition of the 'zero-age' veins; Fig. 9) and partially overlaps the compositional range observed in alkaline OIB. Many alkaline OIB have isotopic compositions that lie within the following ranges: $18 \leq {}^{206}Pb/{}^{204}Pb \leq 20$, $0{\cdot}702 \leq {}^{87}Sr/{}^{86}Sr \leq 0{\cdot}704$, and $0{\cdot}5127 \leq {}^{143}Nd/{}^{144}Nd \leq 0{\cdot}5132$ (as opposed to the more extreme values shown by EM or HIMU basalts), and it is the OIB with these 'normal' isotopic compositions that are consistent with our model of a metasomatized lithospheric source that has evolved for 0·15 Gyr. Significantly, only OIB characterized by EM or HIMU isotopic signatures cannot be explained by the melting of metasomatized lithosphere *in situ*.

In contrast to oceanic settings, the isolation time for metasomatized continental lithosphere could be significantly longer. Figure 9b-I to b-IV shows the isotopic compositional range of metasomatized lithosphere calculated for an isolation time of 0·5 Ga; the figure shows that isolating metasomatized lithosphere for 0·5 Gyr produces a large range of isotope compositions and that this range overlaps the compositions of many continental alkaline basalts. Nevertheless, the isotopic compositions of alkaline continental lavas characterized by high ${}^{87}Sr/{}^{86}Sr$ and low ${}^{206}Pb/{}^{204}Pb$ and ${}^{143}Nd/{}^{144}Nd$ ratios could not be reproduced by the metasomatized lithosphere calculated by our model. However, it is important to note that the isotopic compositions of these basalts may have been modified by interaction with continental crust and/or old lithospheric mantle (Granet *et al.*, 1995; Hoernle *et al.*, 1995; Lustrino & Wilson, 2007). A comparison of the panels in Fig. 9a-I to a-IV and b-I to b-IV indicates that the isolation of metasomatized lithosphere for 0·5 Gyr is not necessary to

reproduce the compositions of continental basalts characterized by $^{206}Pb/^{204}Pb$ isotopic ratios between 19 and 20·5; that is, isolation times of 0·15–0·20 Gyr are sufficient to produce the isotope compositions observed in these continental basalts assuming that the source of the metasomatic veins had an isotopic composition similar to the source of MORB.

Given that the isotopic ratios of the HIMU and EM end-members shown in Fig. 9a-I to a-IV cannot be explained by short times operating on enriched metasomatic veins or metasomatized hydrous lithosphere, we now ask whether longer times might be able to explain these isotopic end-members in the context of our model. Chase (1981), Weaver (1991), and Chauvel *et al.* (1992) have previously suggested that the sources of EM and HIMU lavas have been isolated for long periods of time. If metasomatized lithosphere is recycled through the convecting mantle and entrained in mantle plumes or larger-scale upwellings (e.g. beneath oceanic ridges), then the metasomatic veins characterized by high Rb/Sr, Sm/Nd, and U/Pb would evolve to extreme Sr, Nd, and Pb isotopic signatures if the veins were in fact isolated for time scales of the order of 1–2 Gyr. For example, veins produced from a source composed of 50% E-DMM and 50% DMM with an Sm/Nd ratio of 0·233 (corresponding to the average ratio calculated for our model metasomatized hydrous lithosphere) would develop an ε_{Nd} of −1·67 in 1 Gyr ($^{143}Nd/^{144}Nd = 0{\cdot}512552$). A significant issue for this type of calculation, however, is whether the heterogeneities associated with metasomatized lithosphere (e.g. veins in mantle outcrops in the French Pyrenees are of the order of 0·1–1 m in width) could survive mechanical stirring and diffusive homogenization in the convecting mantle on such time scales (Kogiso *et al.*, 2004*b*). For this reason, we have calculated the isotopic evolution of a source that represents a mixture of 99% depleted mantle (DMM) plus 1% metasomatized hydrous lithosphere (veins plus various proportions of trapped liquid). Figure 9c-I to c-IV shows how the radiogenic isotopic composition of this mixture evolves over 1·5 Gyr (a sample calculation is given in Electronic Appendix B). Our calculations indicate that a large range of isotopic compositions can be produced by isolating the metasomatized lithospheric mantle for ∼1–2 Gyr. These calculations support the idea that recycling in subduction zones or delamination of oceanic and/or continental metasomatized lithosphere could yield enriched mantle with isotopic compositions similar to those inferred for the HIMU end-member.

Figure 9c-I to c-IV also suggests that the isotopic composition of the EM end-member would be difficult to reproduce by long-term isolation of a metasomatic mantle component; the U/Pb ratio calculated for the metasomatized lithosphere is too high to produce the Pb isotopic compositions observed in lavas characterized by EM compositions ($18 < ^{206}Pb/^{204}Pb < 20$) after 1–2 Gyr. To produce such EM compositions from metasomatized lithosphere would require that the hydrous cumulates and associated metasomatic residual liquids were characterized by a slightly higher Rb/Sr ratio (Rb/Sr normalized to PM of ∼1·8) associated with a lower U/Pb ratio (U/Pb normalized to PM of ∼1) than is produced by our model (which starts with mixtures of DMM and E-DMM). These required ratios are outside the range of those calculated for a source composed of 99% DMM plus 1% metasomatized hydrous lithosphere—such ratios have been independently calculated for metasomatized hydrous lithosphere; however, no simulation simultaneously generated a high Rb/Sr [$\sim(1{\cdot}8)_{PM}$] and low U/Pb [$\sim(1)_{PM}$] ratio. An initial source that could potentially produce metasomatic veins with the appropriate Rb/Sr and U/Pb ratios is mantle wedge material that has been enriched by hydrous slab fluids. The presence of such recycled material below mid-ocean ridges has been suggested by Cooper *et al.* (2004) and Donnelly *et al.* (2004) based on oxygen and radiogenic isotope data on MORB from the Mid-Atlantic Ridge, and by Elliott *et al.* (2006) based on the correlation of Li isotope compositions with $^{143}Nd/^{144}Nd$ ratios in MORB from the East Pacific Rise.

It is also possible that the initial melts that fractionate and produce the hydrous cumulates and associated trapped liquid (the equivalent of L_2 in our model) inherited isotopic compositions from their source that are similar to those inferred for HIMU and EM. Although we have assumed that the compositional variability of the asthenospheric source was equivalent to that of DMM and E-DMM (Workman & Hart, 2005), various studies of MORB (Le Roex *et al.*, 1989; Michael, 1995; Niu *et al.*, 1996, 1999; Rehkämper & Hofmann, 1997) have shown that the mid-ocean ridge asthenospheric mantle is more heterogeneous. Ito & Mahoney (2005*a*, 2005*b*) have investigated the melting behaviour of a heterogeneous mantle composed of depleted and enriched components in the context of both MORB and OIB petrogenesis. They concluded that the variations in isotopic composition observed in MORB and OIB are not related to distinct mantle sources for these two suites of basalts, but reflect differences in the depth and extent of melting of MORB and OIB sources. The higher pressures and lower degrees of partial melting allow OIB to retain the more extreme isotopic signatures carried by fertile lithologies in the lithosphere such as recycled oceanic crust or enriched mantle. In contrast, the more extensive low-pressure melting of depleted mantle involved in MORB petrogenesis tends to dilute these extreme isotopic signatures. Their analysis suggests that low-degree melts produced at the periphery of mid-ocean ridges (Fig. 1a) or beneath oceanic or continental lithosphere (Fig. 1b and c) could have more extreme isotopic compositions than we assume in our model. Because both

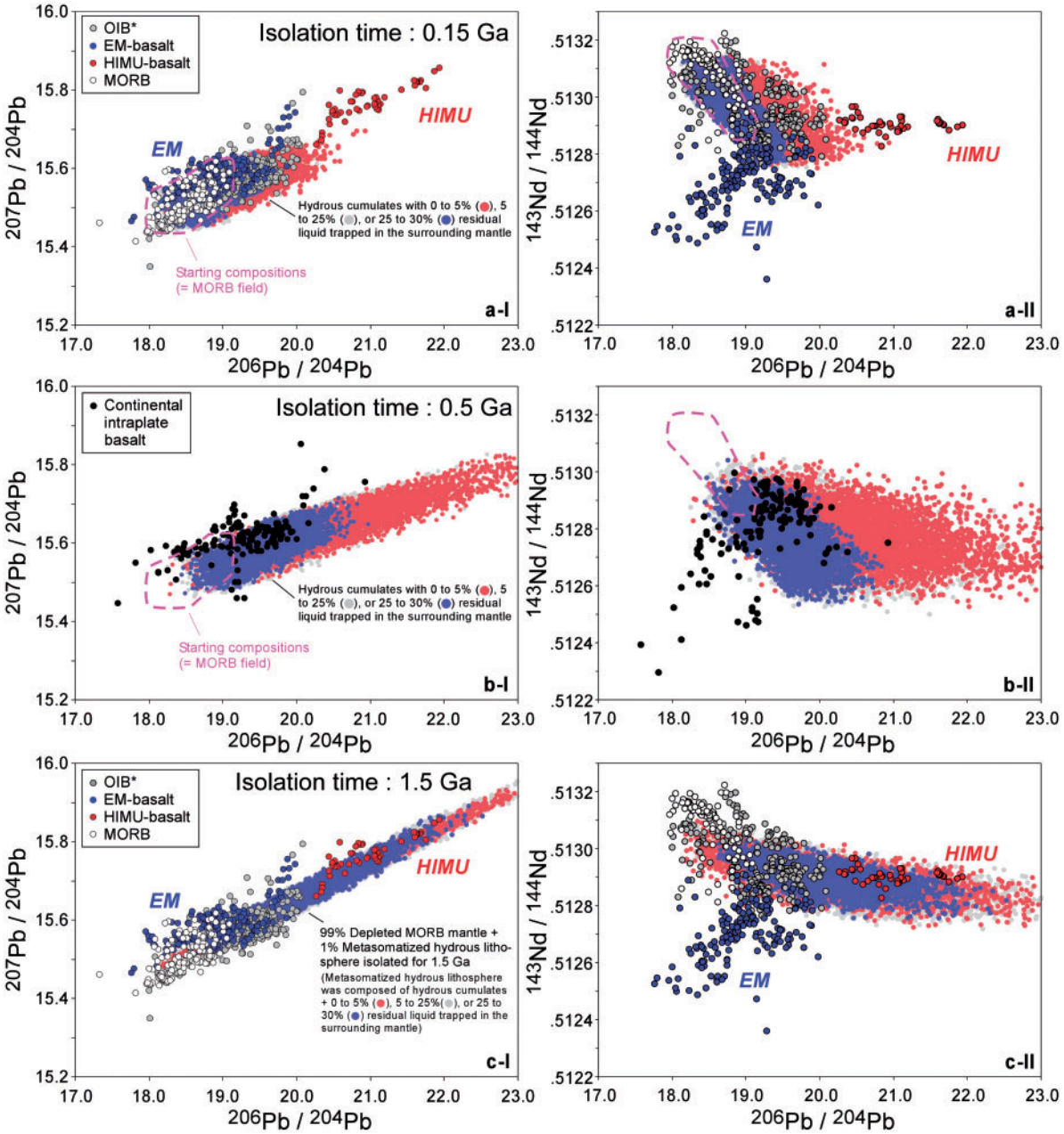

Fig. 9. (a) Isotopic compositions of OIB compared with the calculated isotope ratios of our Monte Carlo model-generated metasomatized hydrous lithosphere (hydrous cumulates plus 0–30% trapped liquid in the surrounding peridotite) isolated for 0·15 Ga. (b) Isotope ratio diagrams for continental alkaline basalts compared with the calculated isotope ratios of metasomatized hydrous lithosphere isolated for 0·5 Ga. (c) Isotope ratio diagrams for OIB compared with the calculated isotopic ratios of metasomatized peridotite (1% metasomatized hydrous lithosphere + 99% depleted mantle) isolated for 1·5 Ga. OIB and continental alkaline basalt data were selected from the GeoRoc database. All rocks are *ne*-normative and have MgO contents between 6 and 20 wt %. HIMU (red dots) and EM (blue dots) basalts are distinguished from 'normal' OIB (OIB*; gray dots) based on their isotopic compositions (EM if $^{143}Nd/^{144}Nd < 0{\cdot}51275$ or $^{87}Sr/^{86}Sr > 0{\cdot}704$; HIMU if $^{206}Pb/^{204}Pb > 20{\cdot}3$; see Fig. 8s–u). MORB data (white circles) are taken from the PetDB database. (See the text and Electronic Appendix B for the details of the calculation.)

silica-deficient and silica-saturated hydrous high-pressure melts evolve towards liquids that crystallize amphiboles with compositions similar to those seen in metasomatic veins (Pilet *et al.*, 2010), the extreme isotopic compositions observed in some islands (e.g. HIMU or EM signatures) could potentially be related to the melting *in situ* of metasomatic veins that represent cumulates from low-degree melts of enriched sources (e.g. recycled lithologies such as

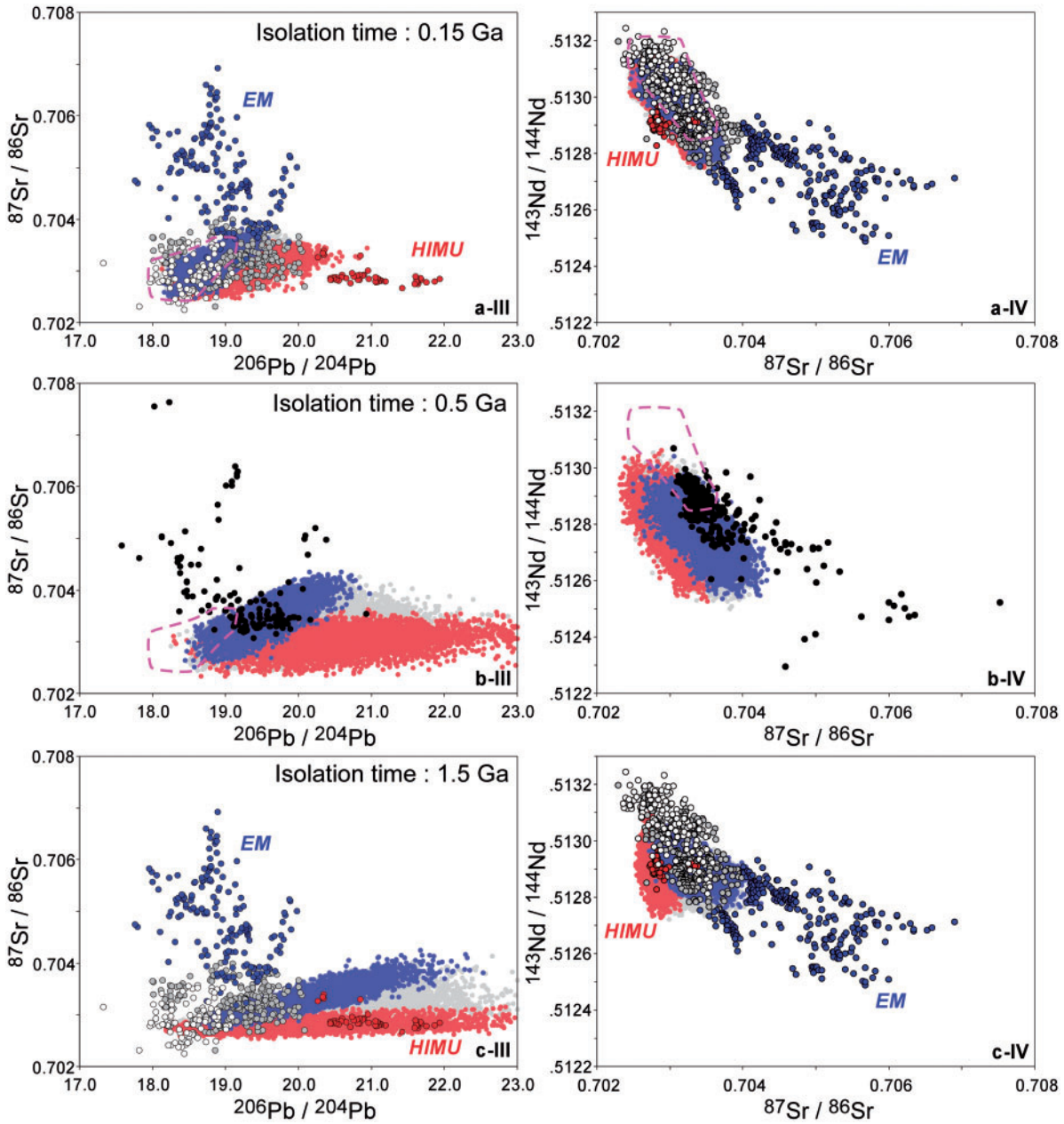

Fig. 9. Continued.

oceanic crust, sediment, or previously metasomatized lithosphere).

CONCLUDING REMARKS

Our Monte Carlo simulations of metasomatic enrichment within the lithosphere show the following results.

(1) The high and fractionated trace-element contents of hydrous metasomatic veins are consistent with these veins representing cumulates produced by fractional crystallization within the lithosphere of low-degree melts from an asthenospheric source similar to that of MORB (i.e. the veins do not represent liquid compositions).

(2) The details of the trace-element patterns observed in these veins (e.g. the positive Nb/La and Ce/Pb ratios; Fig. 5c) are not inherited from the initial low-degree melt of the asthenosphere but instead largely reflect partitioning between amphibole and melt during

fractionation of the mantle-derived melts as they traverse the lithosphere and as amphiboles accumulate in the conduits to form the veins.

(3) Partial melts of the amphibole-rich cumulates based on our models (particularly when the effects of cryptic and modal metasomatism of the peridotitic country rock are included and contribute to the melts) provide good matches to the trace- and minor-element abundances and patterns of basic alkaline magmas (e.g. basanites) from oceanic and continental settings.

(4) Sr, Nd, and Pb radiogenic isotope ratios from time-evolved amphibole-rich cumulates predicted by the Monte Carlo models (+metasomatized adjacent peridotite ± primitive peridotite) are consistent with the range of values observed in most alkaline OIB and continental magmas, although HIMU magmas require *c.* 1–2 Gyr of evolution, and EM magmas cannot be readily explained without appealing to other factors such as a heterogeneous asthenosphere.

These results support the interpretation proposed by various workers that amphibole-bearing veins represent cumulates formed during the differentiation of a volatile-bearing low-degree peridotite melt (e.g. Dawson & Smith, 1982; Nielson & Noller, 1987; Wilshire, 1987; Bodinier *et al.*, 1990; Harte *et al.*, 1993) and that these cumulates are significant components of the sources of alkaline OIB and continental magmas (Lloyd & Bailey, 1975; Wass & Rogers, 1980; Halliday *et al.*, 1990, 1995; McKenzie & O'Nions, 1995; Niu & O'Hara, 2003; Pilet *et al.*, 2005, 2008). Moreover, the results of the forward models provide the potential for detailed tests of this class of hypotheses for the origin of alkaline magmas worldwide and for interpreting major and minor aspects of the geochemical variability of these magmas.

ACKNOWLEDGEMENTS

We thank Paul Asimow, Kurt S. Panter, Julie Prytulak, and an anonymous reviewer for their constructive reviews.

FUNDING

This work was supported by the Swiss National Science Foundation and the University of Lausanne (S.P.), grant PP002-112149 (O.M.), and NSF and DOE grants EAR-0739091 and DE-FG02-06ER15773, respectively (E.M.S.).

SUPPLEMENTARY DATA

Supplementary data for this paper are available at *Journal of Petrology* online.

REFERENCES

Adam, J. & Green, T. (2006). Trace element partitioning between mica- and amphibole-bearing garnet lherzolite and hydrous basanitic melt: l. Experimental results and the investigation of controls on partitioning behavior. *Contributions to Mineralogy and Petrology* **152**, 1–17.

Albarède, F. (1983). Inversion of batch melting equations and the trace-element pattern of the mantle. *Journal of Geophysical Research* **88**, 10573–10583.

Albarède, F. (1995). *Introduction to Geochemical Modeling.* Cambridge: Cambrige University Press.

Asimow, P. D., Dixon, J. E. & Langmuir, C. H. (2004). A hydrous melting and fractionation model for mid-ocean ridge basalts: Application to the Mid-Atlantic Ridge near the Azores. *Geochemistry, Geophysics, Geosystems* **5**, Q01E16, doi:10.1029/2003GC000568.

Aubaud, C., Hauri, E. H. & Hirschmann, M. M. (2004). Hydrogen partition coefficients between nominally anhydrous minerals and basaltic melts. *Geophysical Research Letters* **31**, L20611, doi:10.1029/2004GL021341.

Aubaud, C., Pineau, F., Hékinian, R. & Javoy, M. (2005). Degassing of CO_2 and H_2O in submarine lavas from the Society hotspot. *Earth and Planetary Science Letters* **235**, 511–527.

Baker, M. B., Lesher, C. E. & Stolper, E. M. (2008). Predicting solidus temperatures and modes of mantle peridotites. *Geochimica et Cosmochimica Acta* **72**, A45.

Barling, J. & Goldstein, S. L. (1990). Extreme isotopic variations in Heard Island lavas and the nature of mantle reservoirs. *Nature* **348**, 59–62.

Bea, F., Pereira, M. D. & Stroh, A. (1994). Mineral/leucosome trace-element partitioning in a peraluminous migmatite (a laser ablation-ICP-MS study). *Chemical Geology* **117**, 291–312.

Bedini, R. M. & Bodinier, J.-L. (1999). Distribution of incompatible trace elements between the constituents of spinel peridotite xenoliths: ICP-MS data from the East African Rift. *Geochimica et Cosmochimica Acta* **63**, 3883–3900.

Best, M. G. (1974). Mantle-derived amphibole within inclusions in alkalic-basaltic lavas. *Journal of Geophysical Research* **79**, 2107–2113.

Blundy, J. D., Robinson, J. A. C. & Wood, B. J. (1998). Heavy REE are compatible in clinopyroxene on the spinel lhersolite solidus. *Earth and Planetary Science Letters* **160**, 493–504.

Bodinier, J.-L., Fabriès, J., Lorand, J.-P., Dostal, J. & Dupuy, C. (1987). Geochemistry of amphibole pyroxenite veins from the Lherz and Freychinède ultramafic bodies (Ariège, French Pyrenees). *Bulletin de Minéralogie* **110**, 345–358.

Bodinier, J.-L., Vasseur, G., Vernieres, J., Dupuy, C. & Fabries, J. (1990). Mechanisms of mantle metasomatism: geochemical evidence from the Lherz orogenic peridotite. *Journal of Petrology* **31**, 597–628.

Bodinier, J.-L., Merlet, C., Bedini, R. M., Simien, F., Remaidi, M. & Garrido, C. J. (1996). Distribution of niobium, tantalum, and other highly incompatible trace elements in the lithospheric mantle: The spinel paradox. *Geochimica et Cosmochimica Acta* **60**, 545–550.

Bodinier, J.-L., Menzies, M. A., Shimizu, N., Frey, F. A. & McPherson, E. (2004). Silicate, hydrous and carbonate metasomatism at Lherz, France: Contemporaneous derivatives of silicate melt–harzburgite reaction. *Journal of Petrology* **45**, 299–320.

Cartigny, P., Pineau, F., Aubaud, C. & Javoy, M. (2008). Towards a consistent mantle carbon flux estimate: Insights from volatile systematics (H_2O/Ce, δD, CO_2/Nb) in the North Atlantic mantle (14°N and 34°N). *Earth and Planetary Science Letters* **265**, 672–685.

Chase, C. G. (1981). Oceanic island Pb: Two-stage histories and mantle evolution. *Earth and Planetary Science Letters* **52**, 277–284.

Chauvel, C., Hofmann, A. W. & Vidal, P. (1992). HIMU–EM: The French Polynesian connection. *Earth and Planetary Science Letters* **110**, 99–119.

Class, C. & Goldstein, S. L. (1997). Plume–lithosphere interactions in the ocean basins: constraints from the source mineralogy. *Earth and Planetary Science Letters* **150**, 245–260.

Conquéré, F. (1971). Amphibole pyroxenites and amphibolites associated with lherzolites from Lherz: An example of the effect of water on the fractionation of liquids derived from partial melting of lherzolites. *Contributions to Mineralogy and Petrology* **33**, 32–61.

Conquéré, F. (1977). Petrology of the layered pyroxenites in the ultramafic complexes from Ariège (France) and other occurrences of spinel lherzolites. I. Mineralogical and chemical compositions, evolution of physical equilibrium conditions. *Bulletin de la Société Française de Minéralogie et de Cristallographie* **100**, 42–80.

Cooper, K. M., Eiler, J. M., Asimow, P. D. & Langmuir, C. H. (2004). Oxygen isotope evidence for the origin of enriched mantle beneath the mid-Atlantic ridge. *Earth and Planetary Science Letters* **220**, 297–316.

Dasgupta, R., Hirschmann, M. M. & Stalker, K. (2006). Immiscible transition from carbonate-rich to silicate-rich melts in the 3 GPa melting interval of eclogite + CO_2 and genesis of silica-undersaturated ocean island lavas. *Journal of Petrology* **47**, 647–671.

Dasgupta, R., Hirschmann, M. M. & Smith, N. D. (2007*a*). Partial melting experiments of peridotite + CO_2 at 3 GPa and genesis of alkalic ocean island basalts. *Journal of Petrology* **48**, 2093–2124.

Dasgupta, R., Hirschmann, M. M. & Smith, N. D. (2007*b*). Water follows carbon: CO_2 incites deep silicate melting and dehydration beneath mid-ocean ridges. *Geology* **35**, 135–138.

Dasgupta, R., Jackson, M. G. & Lee, C.-T. A. (2010). Major element chemistry of ocean island basalts—Conditions of mantle melting and heterogeneity of mantle source. *Earth and Planetary Science Letters* **289**, 377–392.

Dawson, J. B. & Smith, J. V. (1982). Upper-mantle amphiboles: a review. *Mineralogical Magazine* **45**, 35–46.

Dixon, J. E., Leist, L., Langmuir, C. & Schilling, J.-G. (2002). Recycled dehydrated lithosphere observed in plume-influenced mid-ocean-ridge basalt. *Nature* **420**, 385–389.

Donnelly, K. E., Goldstein, S. L., Langmuir, C. H. & Spiegelman, M. (2004). Origin of enriched ocean ridge basalts and implications for mantle dynamics. *Earth and Planetary Science Letters* **226**, 347–366.

Downes, H. (2007). Origin and significance of spinel and garnet pyroxenites in the shallow lithospheric mantle: Ultramafic massifs in orogenic belts in Western Europe and NW Africa. *Lithos* **99**, 1–24.

Downes, H., Beard, A. & Hinton, R. (2004). Natural experimental charges: an ion-microprobe study of trace element distribution coefficients in glass-rich hornblendite and clinopyroxenite xenoliths. *Lithos* **75**, 1–17.

Dunn, T. & Sen, C. (1994). Mineral/matrix partition coefficients for orthopyroxene, plagioclase, and olivine in basaltic to andesitic systems: A combined analytical and experimental study. *Geochimica et Cosmochimica Acta* **58**, 717–733.

Eggler, D. H. & Holloway, J. R. (1977). Partial melting of peridotite in the presence of H_2O and CO_2: Principles and review. *Oregon Department of Geology and Mineral Industries Bulletin* **96**, 15–36.

Elliott, T., Thomas, A., Jeffcoate, A. & Niu, Y. (2006). Lithium isotope evidence for subduction-enriched mantle in the source of mid-ocean-ridge basalts. *Nature* **443**, 565–568.

Elliott, T., Blichert-Toft, J., Heumann, A., Koetsier, G. & Forjaz, V. (2007). The origin of enriched mantle beneath São Miguel, Azores. *Geochimica et Cosmochimica Acta* **71**, 219–240.

Fabbrizio, A., Schmidt, M. W., Gunther, D. & Eikenberg, J. (2010). Ra-partitioning between phlogopite and silicate melt and $^{226}Ra/Ba$–$^{230}Th/Ba$ isochrons. *Lithos* **114**, 121–131.

Faul, U. H. (2001). Melt retention and segregation beneath mid-ocean ridges. *Nature* **410**, 920–923.

Frey, F. A. (1983). Rare earth element abundances in upper mantle rocks. In: Henderson, P. (ed.) *Rare Earth Element Geochemistry. Developments in Geochemistry* **2**. Amsterdam: Elsevier, 153–203.

Gaetani, G. A. & Grove, T. L. (1998). The influence of water on melting of mantle peridotite. *Contributions to Mineralogy and Petrology* **131**, 323–346.

Gaetani, G. A., Asimow, P. D. & Stolper, E. M. (2008). A model for rutile saturation in silicate melts with applications to eclogite partial melting in subduction zones and mantle plumes. *Earth and Planetary Science Letters* **272**, 720–729.

Gast, P. W. (1968). Trace element fractionation and the origin of tholeiitic and alkaline magma types. *Geochimica et Cosmochimica Acta* **32**, 1057–1086.

Gast, P. W., Tilton, G. R. & Hedge, C. (1964). Isotopic composition of lead and strontium from Ascension and Gough Islands. *Science* **145**, 1181–1185.

Granet, M., Wilson, M. & Achauer, U. (1995). Imaging a mantle plume beneath the French Massif Central. *Earth and Planetary Sciences Letters* **136**, 281–296.

Grove, T. L., Chatterjee, N., Parman, S. W. & Médard, E. (2006). The influence of H_2O on mantle wedge melting. *Earth and Planetary Science Letters* **249**, 74–89.

Hack, P. J., Nielsen, R. L. & Johnston, A. D. (1994). Experimentally determined rare-earth element and Y partitioning behavior between clinopyroxene and basaltic liquids at pressures up to 20 kbar. *Chemical Geology* **117**, 89–105.

Halliday, A. N., Davidson, J. P., Holden, P., DeWolf, C., Lee, D.-C. & Fitton, J. G. (1990). Trace-element fractionation in plumes and the origin of HIMU mantle beneath the Cameroon line. *Nature* **347**, 523–528.

Halliday, A. N., Davies, G. R., Lee, D.-C., Tommasini, S., Paslick, C. R., Fitton, J. G. & James, D. E. (1992). Lead isotope evidence for young trace element enrichment in the oceanic upper mantle. *Nature* **359**, 623–627.

Halliday, A. N., Lee, D.-C., Tommasini, S., Davies, G. R., Paslick, C. R., Fitton, J. G. & James, D. E. (1995). Incompatible trace elements in OIB and MORB and source enrichment in the sub-oceanic mantle. *Earth and Planetary Science Letters* **133**, 379–395.

Hanchar, J. M. & Watson, E. B. (2003). Zircon saturation thermometry. In: Hanchar, J. M. & Hoskin, W. O. (eds) *Zircon. Mineralogical Society of America and Geochemical Society, Reviews in Mineralogy and Geochemistry* **53**, 89–112.

Hart, S. R. (1988). Heterogeneous mantle domains: signatures, genesis and mixing chronologies. *Earth and Planetary Science Letters* **90**, 273–296.

Hart, S. R. & Dunn, T. (1993). Experimental cpx/melt partitioning of 24 trace elements. *Contributions to Mineralogy and Petrology* **113**, 1–8.

Hart, S. R. & Gaetani, G. A. (2006). Mantle Pb paradoxes: the sulfide solution. *Contributions to Mineralogy and Petrology* **152**, 295–308.

Harte, B., Hunter, R. H. & Kinny, P. D. (1993). Melt geometry, movement and crystallization, in relation to mantle dykes, veins and metasomatism. *Philosophical Transaction of the Royal Society of London, Series A* **342**, 1–21.

Hauri, E. H., Wagner, T. P. & Grove, T. L. (1994). Experimental and natural partitioning of Th, U, Pb and other trace-elements between garnet, clinopyroxene and basaltic melts. *Chemical Geology* **117**, 149–166.

Hirose, K. (1997). Partial melt compositions of carbonated peridotite at 3 GPa and role of CO_2 in alkali-basalt magma generation. *Geophysical Research Letters* **24**, 2837–2840.

Hirose, K. & Kawamoto, T. (1995). Hydrous partial melting of lherzolite at 1 GPa: The effect of H_2O on the genesis of basaltic magmas. *Earth and Planetary Science Letters* **133**, 463–473.

Hirschmann, M. M. & Dasgupta, R. (2009). The H/C ratios of Earth's near-surface and deep reservoirs, and consequences for deep Earth volatile cycles. *Chemical Geology* **262**, 4–16.

Hirschmann, M. M. & Stolper, E. M. (1996). A possible role for garnet pyroxenite in the origin of the 'garnet signature' in MORB. *Contributions to Mineralogy and Petrology* **124**, 185–208.

Hirschmann, M. M., Kogiso, T., Baker, M. B. & Stolper, E. M. (2003). Alkalic magmas generated by partial melting of garnet pyroxenite. *Geology* **31**, 481–484.

Hirth, G. & Kohlstedt, D. L. (1996). Water in the oceanic upper mantle: implications for rheology, melt extraction and the evolution of the lithosphere. *Earth and Planetary Science Letters* **144**, 93–108.

Hoernle, K., Zhang, Y.-S. & Graham, D. (1995). Seismic and geochemical evidence for large-scale mantle upwelling beneath the eastern Atlantic and western and central Europe. *Nature* **374**, 34–39.

Hofmann, A. W. (1997). Mantle geochemistry: the message from oceanic volcanism. *Nature* **385**, 219–229.

Hofmann, A. W. & White, W. M. (1982). Mantle plumes from ancient oceanic crust. *Earth and Planetary Science Letters* **57**, 421–436.

Hofmann, A. W., Jochum, K. P., Seufert, M. & White, W. M. (1986). Nb and Pb in oceanic basalts: new constraints on mantle evolution. *Earth and Planetary Science Letters* **79**, 33–45.

Hoskin, P. W. O. & Schaltegger, U. (2003). The composition of zircon and igneous and metamorphic petrogenesis. In: Hanchar, J. M. & Hoskin, W. O. (eds) *Zircon. Mineralogical Society of America and Geochemical Society, Reviews in Mineralogy and Geochemistry* **53**, 27–62.

Ionov, D. A. & Hofmann, A. W. (1995). Nb–Ta-rich mantle amphiboles and micas: Implications for subduction-related metasomatic trace element fractionations. *Earth and Planetary Science Letters* **131**, 341–356.

Irving, A. J. (1974). Pyroxene-rich ultramafic xenoliths in the Newer basalts of Victoria, Australia. *Neues Jahrbuch für Mineralogie, Abhandlungen* **120**, 147–167.

Ito, G. & Mahoney, J. J. (2005*a*). Flow and melting of a heterogeneous mantle: 1. Method and importance to the geochemistry of ocean island and mid-ocean ridge basalts. *Earth and Planetary Sciences Letters* **230**, 29–46.

Ito, G. & Mahoney, J. J. (2005*b*). Flow and melting of a heterogeneous mantle: 2. Implications for a chemically nonlayered mantle. *Earth and Planetary Science Letters* **230**, 47–63.

Johnson, K. T. M. (1994). Experimental cpx/ and garnet/melt partitioning of REE and other trace elements at high pressures: Petrogenetic implications. *Mineralogical Magazine* **58A**, 454–455.

Johnson, K. T. M. (1998). Experimental determination of partition coefficients for rare earth and high-field-strength elements between clinopyroxene, garnet, and basaltic melt at high pressures. *Contributions to Mineralogy and Petrology* **133**, 60–68.

Katz, R. F., Spiegelman, M. & Langmuir, C. H. (2003). A new parameterization of hydrous mantle melting. *Geochemistry, Geophysics, Geosystems* **4**, 1073, doi:10.1029/2002GC000433.

Keshav, S., Gudfinnsson, G. H., Sen, G. & Fei, Y. (2004). High-pressure melting experiments on garnet clinopyroxenite and the alkalic to tholeiitic transition in ocean-island basalts. *Earth and Planetary Science Letters* **223**, 365–379.

Klimm, K., Blundy, J. D. & Green, T.H. (2008). Trace element partitioning and accessory phase saturation during H_2O-saturated melting of basalt with implications for subduction zone chemical fluxes. *Journal of Petrology* **49**, 523–553.

Kogiso, T., Hirschmann, M. M. & Pertermann, M. (2004*a*). High-pressure partial melting of mafic lithologies in the mantle. *Journal of Petrology* **45**, 2407–2422.

Kogiso, T., Hirschmann, M. M. & Reiners, P. W. (2004*b*). Length scales of mantle heterogeneities and their relationship to ocean island basalt geochemistry. *Geochimica et Cosmochimica Acta* **68**, 345–360.

LaTourrette, T., Hervig, R. L. & Holloway, J. R. (1995). Trace element partitioning between amphibole, phlogopite, and basanite melt. *Earth and Planetary Science Letters* **135**, 13–30.

Le Roex, A. P., Dick, H. J. B. & Fisher, R. L. (1989). Petrology and geochemistry of MORB from 25°E to 46°E along the Southwest Indian Ridge: Evidence for contrasting styles of mantle enrichment. *Journal of Petrology* **30**, 947–986.

Lloyd, F. E. (1981). Upper-mantle metasomatism beneath a continental rift: clinopyroxenes in alkali mafic lavas and nodules from South West Uganda. *Mineralogical Magazine* **44**, 315–323.

Lloyd, F. E. & Bailey, D. K. (1975). Light element metasomatism of the continental mantle: the evidence and the consequences. In: Ahrens, L. H., Dawson, J. B., Duncan, A. R. & Erlank, A. J. (eds) *Physics and Chemistry of the Earth* **9**. Oxford: Pergamon Press, 389–416.

Lorand, J.-P. & Gregoire, M. (2010). Petrogenesis of Fe–Ti oxides in amphibole-rich veins from the Lherz orogenic peridotite (Northeastern Pyrénées, France). *Contributions to Mineralogy and Petrology* **160**, 99–113.

Lundstrom, C. C., Gill, J., Williams, Q. & Perfit, M. R. (1995). Mantle melting and basalt extraction by equilibrium porous flow. *Science* **270**, 1958–1961.

Lustrino, M. & Wilson, M. (2007). The circum-Mediterranean anorogenic Cenozoic igneous province. *Earth-Science Reviews* **81**, 1–65.

Macpherson, C. G., Hilton, D. R., Mertz, D. F. & Dunai, T. J. (2005). Sources, degassing, and contamination of CO_2, H_2O, He, Ne, and Ar in basaltic glasses from Kolbeinsey Ridge, North Atlantic. *Geochimica et Cosmochimica Acta* **69**, 5729–5746.

McDonough, W. F. & Sun, S.-s. (1995). The composition of the Earth. *Chemical Geology* **120**, 223–253.

McKenzie, D. (1989). Some remarks on the movement of small melt fractions in the mantle. *Earth and Planetary Science Letters* **95**, 53–72.

McKenzie, D. & O'Nions, R. K. (1991). Partial melt distributions from inversion of rare earth element concentrations. *Journal of Petrology* **32**, 1021–1091.

McKenzie, D. & O'Nions, R. K. (1995). The source regions of ocean island basalts. *Journal of Petrology* **36**, 133–159.

McPherson, E., Thirlwall, M. F., Parkinson, I. J., Menzies, M. A., Bodinier, J.-L., Woodland, A. & Bussod, G. (1996). Geochemistry of metasomatism adjacent to amphibole-bearing veins in the Lherz peridotite massif. *Chemical Geology* **134**, 135–157.

Menzies, M. (1983). Mantle ultramafic xenoliths in alkaline magmas: evidence for mantle heterogeneity modified by magmatic activity. In: Hawkesworth, C. J. & Norry, M. J. (eds) *Continental Basalts and Mantle Xenoliths*. Nantwich: Shiva, pp. 92–110.

Michael, P. (1995). Regionally distinctive sources of depleted MORB: Evidence from trace elements and H_2O. *Earth and Planetary Science Letters* **131**, 301–320.

Minster, J. F. & Allègre, C. J. (1978). Systematic use of trace elements in igneous processes Part III: Inverse problem of batch partial melting in volcanic suites. *Contributions to Mineralogy and Petrology* **68**, 37–52.

Minster, J. F., Minster, J. B., Treuil, M. & Allègre, C. J. (1977). Systematic use of trace elements in igneous processes. Part II.

Inverse problem of fractional crystallization process in volcanic suites. *Contributions to Mineralogy and Petrology* **61**, 49–77.

Moine, B. N., Grégoire, M., O'Reilly, S. Y., Sheppard, S. M. F. & Cottin, J. Y. (2001). High field strength element fractionation in the upper mantle: Evidence from amphibole-rich composite mantle xenoliths from the Kerguelen Islands (Indian Ocean). *Journal of Petrology* **42**, 2145–2167.

Morris, E. M. & Pasteris, J. D. (eds) (1987). *Mantle Metasomatism and Alkaline Magmatism. Geological Society of America, Special Papers* **215**.

Müntener, O. & Ulmer, P. (2006). Experimentally derived high-pressure cumulates from hydrous arc magmas and consequences for the seismic velocity structure of lower arc crust. *Geophysical Research Letters* **33**, L21308, doi:10.1029/2006GL027629.

Müntener, O., Kelemen, P. B. & Grove, T. L. (2001). The role of H_2O during crystallization of primitive arc magmas under uppermost mantle conditions and genesis of igneous pyroxenites: an experimental study. *Contributions to Mineralogy and Petrology* **141**, 643–658.

Nakamura, Y. & Tatsumoto, M. (1988). Pb, Nd, and Sr isotopic evidence for a multicomponent source for rocks of Cook–Austral Islands and heterogeneities of mantle plumes. *Geochimica et Cosmochimica Acta* **52**, 2909–2924.

Nekvasil, H., Dondolini, A., Horn, J., Filiberto, J., Long, H. & Lindsley, D. H. (2004). The origin and evolution of silica-saturated alkalic suites: an experimental study. *Journal of Petrology* **45**, 693–721.

Nielson, J. E. & Noller, J. S. (1987). Processes of mantle metasomatism; Constraints from observations of composite peridotite xenoliths. In: Morris, E. M. & Pasteris, J. D. (eds) *Mantle Metasomatism and Alkaline Magmatism. Geological Society of America, Special Papers* **215**, 61–76.

Nielson, J. E. & Wilshire, H. G. (1993). Magma transport and metasomatism in the mantle: A critical review of current geochemical models. *American Mineralogist* **78**, 1117–1134.

Nielson, J. E., Budahn, J. R., Unruh, D. M. & Wilshire, H. G. (1993). Actualistic models of mantle metasomatism documented in a composite xenolith from Dish Hill, California. *Geochimica et Cosmochimica Acta* **57**, 105–121.

Niu, Y. & O'Hara, M. J. (2003). Origin of ocean island basalts: A new perspective from petrology, geochemistry, and mineral physics considerations. *Journal of Geophysical Research* **108**, 2209, doi:10.1029/2002JB002048.

Niu, Y., Waggoner, D. G., Sinton, J. M. & Mahoney, J. J. (1996). Mantle source heterogeneity and melting processes beneath seafloor spreading centers: The East Pacific Rise, 18°–19° S. *Journal of Geophysical Research* **101**, 27711–27733.

Niu, Y., Collerson, K. D., Batiza, R., Wendt, J. I. & Regelous, M. (1999). Origin of enriched-type mid-ocean ridge basalt at ridges far from mantle plumes: The East Pacific Rise at 11° 20′ N. *Journal of Geophysical Research* **104**, 7067–7087.

Palacz, Z. A. & Saunders, A. D. (1986). Coupled trace element and isotope enrichment in the Cook–Austral–Samoa islands, southwest Pacific. *Earth and Planetary Science Letters* **79**, 270–280.

Panter, K. S., Blusztajn, J., Hart, S. R., Kyle, P. R., Esser, R. & McIntosh, W. C. (2006). The origin of HIMU in the SW Pacific: Evidence from intraplate volcanism in southern New Zealand and subantarctic islands. *Journal of Petrology* **47**, 1673–1704.

Pichavant, M., Montel, J.-M. & Richard, L. R. (1992). Apatite solubility in peraluminous liquids: Experimental data and an extension of the Harrison–Watson model. *Geochimica et Cosmochimica Acta* **56**, 3855–3861.

Pilet, S., Hernandez, J., Bussy, F. & Sylvester, P. J. (2004). Short-term metasomatic control of Nb/Th ratios in the mantle sources of intraplate basalts. *Geology* **32**, 113–116.

Pilet, S., Hernandez, J., Sylvester, P. & Poujol, M. (2005). The metasomatic alternative for ocean island basalt chemical heterogeneity. *Earth and Planetary Science Letters* **236**, 148–166.

Pilet, S., Baker, M. B. & Stolper, E. M. (2008). Metasomatized lithosphere and the origin of alkaline lavas. *Science* **320**, 916–919.

Pilet, S., Ulmer, P. & Villiger, S. (2010). Liquid line of descent of a basanitic liquid at 1·5 GPa: constraints on the formation of metasomatic veins. *Contributions to Mineralogy and Petrology* **159**, 621–643.

Pineau, F., Shilobreeva, S., Hekinian, R., Bideau, D. & Javoy, M. (2004). Deep-sea explosive activity on the Mid-Atlantic Ridge near 34° 50′ N: a stable isotope (C, H, O) study. *Chemical Geology* **211**, 159–175.

Prytulak, J. & Elliott, T. (2007). TiO_2 enrichment in ocean island basalts. *Earth and Planetary Science Letters* **263**, 388–403.

Rehkämper, M. & Hofmann, A. W. (1997). Recycled ocean crust and sediment in Indian Ocean MORB. *Earth and Planetary Science Letters* **147**, 93–106.

Robinson, J. A. C. & Wood, B. J. (1998). The depth of the spinel to garnet transition at the peridotite solidus. *Earth and Planetary Science Letters* **164**, 277–284.

Roden, M. K., Hart, S. R., Frey, F. A. & Melson, W. G. (1984). Sr, Nd and Pb isotopic and REE geochemistry of St. Paul's Rocks: the metamorphic and metasomatic development of an alkali basalt mantle source. *Contributions to Mineralogy and Petrology* **85**, 376–390.

Saal, A. E., Hauri, E. H., Langmuir, C. H. & Perfit, M. R. (2002). Vapour undersaturation in primitive mid-ocean-ridge basalt and the volatile content of Earth's upper mantle. *Nature* **419**, 451–455.

Salters, V. J. M. & Longhi, J. (1999). Trace element partitioning during the initial stages of melting beneath mid-ocean ridges. *Earth and Planetary Science Letters* **166**, 15–30.

Salters, V. J. M. & Stracke, A. (2004). Composition of the depleted mantle. *Geochemistry, Geophysics, Geosystems* **5**, Q05004, doi:10.1029/2003GC000597.

Shaw, A. M., Behn, M. D., Humphris, S. E., Sohn, R. A. & Gregg, P. M. (2010). Deep pooling of low degree melts and volatile fluxes at the 85° E segment of the Gakkel Ridge: Evidence from olivine-hosted melt inclusions and glasses. *Earth and Planetary Science Letters* **289**, 311–322.

Shcheka, S. S., Wiedenbeck, M., Frost, D. J. & Keppler, H. (2006). Carbon solubility in mantle minerals. *Earth and Planetary Science Letters* **245**, 730–742.

Simons, K., Dixon, J., Schilling, J.-G., Kingsley, R. & Poreda, R. (2002). Volatiles in basaltic glasses from the Easter–Salas y Gomez Seamount Chain and Easter Microplate: Implications for geochemical cycling of volatile elements. *Geochemistry, Geophysics, Geosystems* **3**, 1039, doi:10.1029/2001GC000173.

Sims, K. W. W. & DePaolo, D. J. (1997). Inferences about mantle magma sources from incompatible element concentration ratios in oceanic basalts. *Geochimica et Cosmochimica Acta* **61**, 765–784.

Sisson, T. W. & Grove, T. L (1993). Experimental investigations of the role of H_2O in calc-alkaline differentiation and subduction zone magmatism. *Contributions to Mineralogy and Petrology* **113**, 143–166.

Sobolev, A. V. & Chaussidon, M. (1996). H_2O concentrations in primary melts from supra-subduction zones and mid-ocean ridges: Implications for H_2O storage and recycling in the mantle. *Earth and Planetary Science Letters* **137**, 45–55.

Stolper, E. & Asimow, P. (2007). Insights into mantle melting from graphical analysis of one-component systems. *American Journal of Science* **307**, 1051–1139.

Stracke, A. & Bourdon, B. (2009). The importance of melt extraction for tracing mantle heterogeneity. *Geochimica et Cosmochimica Acta* **73**, 218–238.

Stracke, A., Bizimis, M. & Salters, V. J. M. (2003). Recycling oceanic crust: Quantitative constraints. *Geochemistry, Geophysics, Geosystems* **4**, 8003, doi:10.1029/2001GC000223.

Sun, S.-s. & McDonough, W. F. (1989). Chemical and isotopic systematics of oceanic basalts: implications for mantle composition and processes. In: Saunders, A. D. & Norry, M. J. (eds) *Magmatism in the Ocean Basins. Geological Society, London, Special Publications* **42**, 313–345.

Thompson, R. N., Ottley, C. J., Smith, P. M., Pearson, D. G., Dickin, A. P., Morrison, M. A., Leat, P. T. & Gibson, S. A. (2005). Source of the Quaternary alkalic basalts, picrites and basanites of the Potrillo Volcanic Field, New Mexico, USA: Lithosphere or convecting mantle? *Journal of Petrology* **46**, 1603–1643.

Tiepolo, M., Vannucci, R., Bottazzi, P., Oberti, R., Zanetti, A. & Foley, S. (2000*a*). Partitioning of rare earth elements, Y, Th, U, and Pb between pargasite, kaersutite, and basanite to trachyte melts: Implications for percolated and veined mantle. *Geochemistry, Geophysics, Geosystems* **1**, paper number 2000GC000064.

Tiepolo, M., Vannucci, R., Oberti, R., Foley, S., Bottazzi, P. & Zanetti, A. (2000*b*). Nb and Ta incorporation and fractionation in titanian pargasite and kaersutite: crystal-chemical constraints and implications for natural systems. *Earth and Planetary Science Letters* **176**, 185–201.

Tiepolo, M., Oberti, R., Zanetti, A., Vannucci, R. & Foley, S. (2007). Trace-element partitioning between amphibole and silicate melt. In: Hawthorne, F. C., Oberti, R., Ventura, G. D. & Mottana, A. (eds) *Amphiboles: Crystal Chemistry, Occurrence, and Health Issues. Mineralogical Society of America and Geochemical Society, Reviews in Mineralogy and Geochemistry* **67**, 417–452.

van Westrenen, W., Blundy, J. D. & Wood, B. J. (2000). Effect of Fe^{2+} on garnet–melt trace element partitioning: experiments in FCMAS and quantification of crystal-chemical controls in natural systems. *Lithos* **53**, 189–201.

Varne, R. (1970). Hornblende lherzolite and the upper mantle. *Contributions to Mineralogy and Petrology* **27**, 45–51.

Vaselli, O., Downes, H., Thirlwall, M., Dobosi, G., Coradossi, N., Seghedi, I., Szakacs, A. & Vannucci, R. (1995). Ultramafic xenoliths in Plio-Pleistocene alkali basalts from the eastern Transylvanian Basin: Depleted mantle enriched by vein metasomatism. *Journal of Petrology* **36**, 23–53.

Villemant, B. (1985). La différentiation des séries volcaniques: Géochimie des éléments traces dans les séries du Massif Central et d'Italie Centrale, Thèse doctorat d'Etat es Sciences Naturelles, Université Pierre et Marie Curie.

Walter, M. J. (1998). Melting of garnet peridotite and the origin of komatiite and depleted lithosphere. *Journal of Petrology* **39**, 29–60.

Wass, S. Y. & Rogers, N. W. (1980). Mantle metasomatism—precursor to continental alkaline volcanism. *Geochimica et Cosmochimica Acta* **44**, 1811–1823.

Weaver, B. L. (1991). The origin of ocean island basalt end-member compositions: trace-element and isotopic constraints. *Earth and Planetary Science Letters* **104**, 381–397.

Willbold, M. & Stracke, A. (2006). Trace element composition of mantle end-members: Implications for recycling of oceanic and upper and lower continental crust. *Geochemistry, Geophysics, Geosystems* **7**, Q04004, doi:10.1029/2005GC001005.

Wilshire, H. G. (1987). A model of mantle metasomatism. In: Morris, E. M. & Pasteris, J. D. (eds) *Mantle Metasomatism and Alkaline Magmatism. Geological Society of America, Special Papers* **215**, 47–60.

Wilshire, H. G., Nielson Pike, J. E., Meyer, C. E. & Schwarzman, E. C. (1980). Amphibole-rich veins in lherzolite xenoliths, Dish Hill and Deadman Lake, California. *American Journal of Science* **280-A**, 576–593.

Wilson, M. & Patterson, R. (2001). Intraplate magmatism related to short-wavelength convective instabilities in the upper mantle: Evidence from the Tertiary–Quaternary volcanic province of western and central Europe. In: Ernst, R. E. & Buchan, K. L. (eds) *Mantle Plumes: their Identification through Time. Geological Society of America, Special Papers* **352**, 37–58.

Woodland, A. B., Kornprobst, K., McPherson, E., Bodinier, J.-L. & Menzies, M. A. (1996). Metasomatic interactions in the lithospheric mantle: petrologic evidence from the Lherz massif, French Pyrenees. *Chemical Geology* **134**, 83–112.

Workman, R. K. & Hart, S. R. (2005). Major and trace element composition of the depleted MORB mantle (DMM). *Earth and Planetary Science Letters* **231**, 53–72.

Workman, R. K., Hart, S. R., Jackson, M., Regelous, M., Farley, K. A., Blusztajn, J., Kurz, M. & Staudigel, H. (2004). Recycled metasomatized lithosphere as the origin of the enriched mantle II (EM2) end-member: Evidence from the Samoan Volcanic Chain. *Geochemistry, Geophysics, Geosystems* **5**, Q04008, doi:10.1029/2003GC000623.

Wulff-Pedersen, E., Neumann, E.-R., Vannucci, R., Bottazzi, P. & Ottolini, L. (1999). Silicic melts produced by reaction between peridotite and infiltrating basaltic melts: ion probe data on glasses and minerals in veined xenoliths from La Palma, Canary Islands. *Contributions to Mineralogy and Petrology* **137**, 59–82.

Wyllie, P. J. (1977). Mantle fluid compositions buffered by carbonates in peridotite–CO_2–H_2O. *Journal of Geology* **85**, 187–207.

Wyllie, P. J. (1988*a*). Magma genesis, plate tectonics, and chemical differentiation of the Earth. *Reviews of Geophysics* **26**, 370–404.

Wyllie, P. J. (1988*b*). Solidus curves, mantle plumes, and magma generation beneath Hawaii. *Journal of Geophysical Research* **93**, 4171–4181.

Zack, T. & Brumm, R. (1998). Ilmenite/liquid partition coefficients of 26 trace elements determined through ilmenite/clinopyroxene partitioning in garnet pyroxenite. In: Gurney, J. J., Gurney, J. L., Pascoe, M. D. & Richardson, S. H. (eds) *7th International Kimberlite Conference*. Cape Town: Red Roof Design, pp. 986–988.

Zanetti, A., Vannucci, R., Bottazzi, P., Oberti, R. & Ottolini, L. (1996). Infiltration metasomatism at Lherz as monitored by systematic ion-microprobe investigations close to a hornblendite vein. *Chemical Geology* **134**, 113–133.

Zindler, A. & Hart, S. (1986). Chemical geodynamics. *Annual Review of Earth and Planetary Sciences* **14**, 493–571.